

AWARD NUMBER: W81XWH-05-1-0592

TITLE: PSMA-Targeted Nano-Conjugates as Dual-Modality (MRI/PET) Imaging Probes for the Non-Invasive Detection of Prostate Cancer

PRINCIPAL INVESTIGATOR: Xiankai Sun, Ph.D.

CONTRACTING ORGANIZATION: Texas Southwestern Medical Center
Dallas, Texas 75390

REPORT DATE: October 2009

TYPE OF REPORT: Final

PREPARED FOR: U.S. Army Medical Research and Materiel Command
Fort Detrick, Maryland 21702-5012

DISTRIBUTION STATEMENT: Approved for Public Release;
Distribution Unlimited

The views, opinions and/or findings contained in this report are those of the author(s) and should not be construed as an official Department of the Army position, policy or decision unless so designated by other documentation.

REPORT DOCUMENTATION PAGE			<i>Form Approved</i> <i>OMB No. 0704-0188</i>		
Public reporting burden for this collection of information is estimated to average 1 hour per response, including the time for reviewing instructions, searching existing data sources, gathering and maintaining the data needed, and completing and reviewing this collection of information. Send comments regarding this burden estimate or any other aspect of this collection of information, including suggestions for reducing this burden to Department of Defense, Washington Headquarters Services, Directorate for Information Operations and Reports (0704-0188), 1215 Jefferson Davis Highway, Suite 1204, Arlington, VA 22202-4302. Respondents should be aware that notwithstanding any other provision of law, no person shall be subject to any penalty for failing to comply with a collection of information if it does not display a currently valid OMB control number. PLEASE DO NOT RETURN YOUR FORM TO THE ABOVE ADDRESS.					
1. REPORT DATE 1 October 2009		2. REPORT TYPE Final		3. DATES COVERED 15 Sep 2006 – 14 Sep 2009	
4. TITLE AND SUBTITLE PSMA-Targeted Nano-Conjugates as Dual-Modality (MRI/PET) Imaging Probes for the Non-Invasive Detection of Prostate Cancer			5a. CONTRACT NUMBER		
			5b. GRANT NUMBER W81XWH-05-1-0592		
			5c. PROGRAM ELEMENT NUMBER		
6. AUTHOR(S) Xiankai Sun, Ph.D. E-Mail: Xiankai.Sun@UTSouthwestern.edu			5d. PROJECT NUMBER		
			5e. TASK NUMBER		
			5f. WORK UNIT NUMBER		
7. PERFORMING ORGANIZATION NAME(S) AND ADDRESS(ES) Texas Southwestern Medical Center Dallas, Texas 75390			8. PERFORMING ORGANIZATION REPORT NUMBER		
9. SPONSORING / MONITORING AGENCY NAME(S) AND ADDRESS(ES) U.S. Army Medical Research and Materiel Command Fort Detrick, Maryland 21702-5012			10. SPONSOR/MONITOR'S ACRONYM(S)		
			11. SPONSOR/MONITOR'S REPORT NUMBER(S)		
12. DISTRIBUTION / AVAILABILITY STATEMENT Approved for Public Release; Distribution Unlimited					
13. SUPPLEMENTARY NOTES					
14. ABSTRACT The goal of this project is to develop dual modality imaging probes for the detection of prostate cancer by doping radioisotopes to iron oxide nanoparticles, so that the sensitivity and specificity of prostate cancer diagnosis could be significantly improved. During the funding period, a facile approach was developed to prepare gamma- or positron emitting nuclides incorporated SPIO nanoparticles (NUSPIONS) for dual modality imaging of prostate cancer. Preliminary MR and autoradiography images with ¹⁷⁷ Lu-NUSPIONS in nude mice bearing PC-3 tumors clearly showed tumors implanted in the flanks, indicating the potential application of such nanoplatfroms for the noninvasive dual modality imaging of prostate cancer. Due to the limited availability of As-74 in the USA, this novel approach was applied to another nanoplatfrom, gold nanoparticle (AuNP), for the development of multi-modality imaging probes for prostate cancer detection. The AuNP-based multi-modality nanoprobos showed great potential in non-invasive detection of distal prostate cancer metastases in an orthotopic tumor model. Furthermore, a PET/CT dual modality nanoprobe was prepared by incorporating a positron emitter (Cu-64) instead of As-74 into the core of AuNPs and the probe was able to reveal the nevasculature formation of tumor in a prostate cancer mouse model on PET/CT images.					
15. SUBJECT TERMS None provided.					
16. SECURITY CLASSIFICATION OF:			17. LIMITATION OF ABSTRACT	18. NUMBER OF PAGES	19a. NAME OF RESPONSIBLE PERSON USAMRMC
a. REPORT U	b. ABSTRACT U	c. THIS PAGE U			19b. TELEPHONE NUMBER (include area code)
			UU	36	

Table of Contents

Introduction.....	3
Body.....	3
Key Research Accomplishments.....	17
Reportable Outcomes.....	17
Conclusions.....	18
References.....	18
Appendices.....	19-36

Introduction

The goal of this project was set to explore a new approach that will combine the advantages of MRI and PET for the diagnostic imaging and staging of prostate cancer. We propose to dope positron-emitting isotopes to superparamagnetic iron oxide nanoparticle to make nanosized dual MRI/PET probes for the detection of prostate cancer by multi-modality (anatomical MRI plus functional PET) molecular imaging approaches, so that the sensitivity and specificity of prostate cancer diagnosis could be significantly improved. To realize the goal, two objectives were specified for this project: **Objective I.** Preparation/characterization of $^{77/74}\text{As}$ -doped iron oxide nanoparticles and construction of PSMA-targeted nano-conjugates; and **Objective II.** Evaluation of the PSMA-targeted nano-conjugates in prostate cancer xenograft mouse models via conventional biodistribution and small animal MRI/PET imaging methods.

Body

In the statement of work (SOW) of this project, the milestones and timelines were arranged in order to achieve the two Objectives:

Objective I.

Months 0 – 12:

Milestone: Establish protocols of making dextran-coated iron oxide nanoparticles. We anticipate to obtaining optimal conditions to control the size of nanoparticles in range of 20 – 40 nm within the first year.

Accomplished: Please see my 1st annual report.

Months 6 – 15:

Milestone: Establish protocols of making dextran-coated $^{77/74}\text{As}$ -doped iron oxide nanoparticles.

Accomplished: Please see my 1st and 2nd annual reports.

Months 9 – 18:

Milestone: Establish protocols to construct PSMA-targeted nano-conjugates. Four such nano-conjugates are anticipated (two nano-conjugates with sizes of 25 nm and 35 nm per targeting molecule).

Accomplished: Please see my 1st, 2nd, and 3rd annual reports.

Objective II.

Months 12 – 30:

Milestone: Accomplish the in vitro/in vivo evaluations of the four PSMA-targeted nano-conjugates. At the end of this timeframe, we will be able to tell which targeting approach is better. We anticipate two nano-conjugates (one per targeting molecule) that can be used for small animal imaging studies.

Partially completed: Please see my 3rd annual report

Months 24 - 36:

Milestone: Accomplish the small animal MRI and PET imaging evaluation of the two chosen nano-conjugates. We anticipate that the PSMA-targeted nano-conjugates can serve as dual-modality imaging

probes, which will provide the desired higher sensitivity and specificity for PCa detection than either of the single-modality imaging approaches and the PSA test, by the combined analysis of MRI and PET images.

Partially completed: Please see my 3rd annual report

The key accomplishments using dextran-coated iron oxide nanoparticles were detailed in my 3rd annual report.

The main obstacle that we have met in carrying out this project is the availability of As-74 in the USA. Therefore instead of using As-74, we applied our developed approach in the 1st – 3rd year of the project to the following two sub-projects, which were intended to achieve the same Objectives but using a different nanoplatform (Gold Nanoparticle) and a different positron emitter, Cu-64. The rationale of using this nanoplatform will be detailed later.

- i) Gold nanoparticle based CT/SERS Nanoprobes for the detection of prostate cancer metastases
- ii) Cu-64 incorporated gold nanoparticles as dual modality (PET/CT) imaging agents for prostate cancer detection

The two sub-projects have been progressing very well.

i) Gold nanoparticle based CT/SERS Nanoprobes for the detection of prostate cancer metastases

RATIONALE:

Development of nanoparticle based contrast agents for diagnostic imaging applications is currently a very active area of research. Over the past decade, a wide variety of materials have been used to synthesize nanoparticle based contrast agents/beacons for in vitro and in vivo imaging applications. Although many different types (geometry and material) of nanoparticles have shown promising results for imaging in an in vitro setting, using them in vivo is limited by the constraints related to size, shape surface chemistry and cyto-toxicity. Given these constraints, only a small set of nanoparticles have the potential to be used for in vivo diagnostic imaging applications which include metal and polymer nanoparticles. Metal nanoparticles have been exploited to enhance contrast of imaging modalities which include MRI, CT, ultrasound and optical. Furthermore, metal nanoparticles exhibit unique electromagnetic properties such as enhanced fluorescence and Raman scattering that can be exploited to improve sensitivity and multiplexed molecular imaging. Gold nanoparticles (AuNPs) in particular are well suited for in vivo imaging applications given their low toxicity and reactive surface that is conducive for bioconjugation using the thiol chemistry. AuNPs provide a robust platform for the development of functionalized contrast agents for diagnostic molecular imaging applications.

Multi-modality contrast agents can combine the complementary strengths of different imaging modalities to enable comprehensive diagnostic imaging for pathologies such as cancer. Imaging modalities such as CT and MRI enable whole body imaging with high resolution but lack the sensitivity that can be achieved by optical techniques which in turn have limited penetration depth and interrogation volume. Regardless of the imaging technique, the weak endogenous contrast between normal and abnormal tissue necessitates the development and use of exogenous contrast agents for diagnostic imaging. Even biopsied ex vivo tissue samples have to be stained with multiple contrast agents to obtain a comprehensive molecular and morphological profile for accurate clinical diagnosis. AuNPs assisted improvement in contrast and sensitivity for CT and optical imaging has been demonstrated. A nanoparticle probe that can simultaneously enhance the contrast of CT and optical imaging modality such as Raman spectroscopy can

potentially be very valuable for many diagnostic imaging applications. Dual-modality probes for combined MRI and fluorescence imaging using iron oxide nanoparticles have been demonstrated.

Raman spectroscopy is a highly sensitive technique for molecular detection since every molecule has a unique spectral fingerprint known as its Raman spectrum. A major weakness of Raman spectroscopy is the poor efficiency of Raman scattering which has limited its use in biomedical applications. Efficiency of Raman scattering can dramatically increase (enhancement factor - 10^6 to 10^{14}) when a molecule of interest is in close proximity to a nanosurface via phenomenon known as surface enhanced Raman scattering. With such large enhancement of Raman scattering the use of surface enhanced Raman spectroscopy (SERS) for imaging application is an attractive alternative to fluorescence. Fluorescent tags have emerged as dominant optical contrast agents for molecular imaging for a wide variety of in vitro applications. In vivo applications of organic fluorescent dyes have been limited due to auto-fluorescence of tissue. Recently developed near infrared fluorescent dyes do reduce the auto-fluorescence but still fluorescence tags fundamentally suffer from photo-bleaching and limited colors (two or three) that can be simultaneously detected due to spectral overlap. These limitations can be overcome by SERS to achieve the detection sensitivity that potentially exceeds that of fluorescence techniques and also achieve quantitative multiplexed detection of several biomolecules simultaneously.

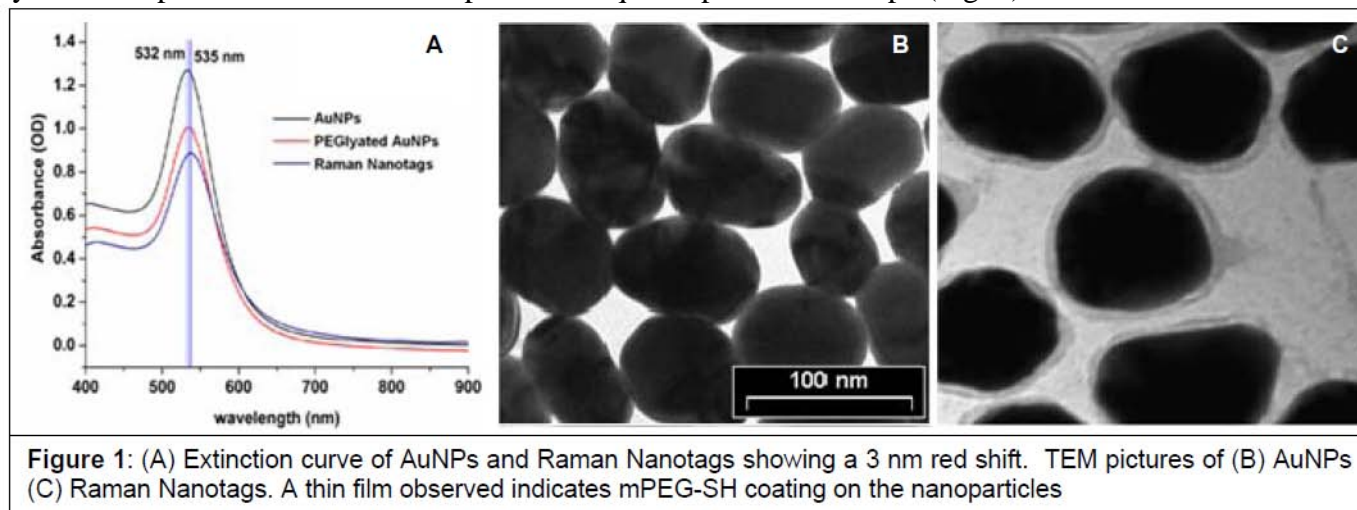
Despite the unique advantages offered by SERS, lack of signal reproducibility and quantification has prevented its wide spread use for in vitro or in vivo imaging applications until now. The lack of signal reproducibility can occur due to the variation in nanoparticle size and distribution or aggregation. Metal nanoparticles tend to aggregate in commonly used buffers and serum. Although aggregation enhances the SERS signal but from a practical standpoint it is undesirable since aggregation cannot be controlled, resultant SERS signal fluctuates, and the aggregate size is too large to be used for any in vivo applications. Recently a promising design strategy to synthesize Nanotags for SERS has been developed. The design involves encapsulating organic dyes as signature reporter dye between AuNP and a layer of silica or PEG. Specific target ligands can be attached to PEG or silica surface with well established bioconjugation chemistries. CT is a widely used imaging modality for various clinical diagnostic applications. Hard tissues have higher X-ray attenuations than various soft tissues whereas the contrast between soft tissues is inherently poor, which limits the sensitivity with which diagnosis of pathologies such as cancer can be made. Currently, iodine based compounds are used to enhance contrast of CT which have the limitations of short imaging window due to rapid clearance by kidneys and renal toxicity. Metals such as gold have a larger X-ray attenuation coefficient due to their high electron density and atomic number compared to conventionally used iodine compounds. Nanoparticle based CT contrast agents have been demonstrated for vascular imaging, which include, bare AuNPs, polymer-coated AuNPs, gadolinium-coated AuNPs and polymer-coated Bi_2S_3 . Molecular CT imaging of cancer using targeted AuNPs in cell culture has been demonstrated by Popovtzer et. al.

Combined CT imaging and SERS enabled by a single probe has not been demonstrated yet. As such, we set out to develop dual-modality contrast agents for combined CT and SERS imaging. The hybrid nanotags are quasi-spherical gold nanoparticles coated with a Raman reporter dye (color) encapsulated by a monolayer of polyethylene glycol (PEG) molecules with carboxylate functional group for further bioconjugation with a ligand.

Accomplished Work

Synthesis of Nanotags: Size and shape of metal nanoparticles are critical factors that influence the enhancement of Raman scattering. AuNPs of different sizes were employed as the cores to construct Nanotags. The AuNPs were synthesized using published methods with modifications. In brief, to prepare citrate coated AuNPs, an aqueous solution of 0.25 mM HAuCl_4 (50 mL) was first heated to boiling with constant stirring, to which a certain volume of 1% (wt) sodium citrate (0.40 – 1.75 mL) was added. Within a minute, the solution turned from faint blue to red indicating the formation of AuNPs. The boiling and

stirring were continued for 30 min. The resulting solution was then cooled down to room temperature, which afforded AuNPs with a mean diameter ranging from 16.7 ± 1.7 nm to 65.6 ± 6.4 nm as determined by TEM. In this method, the particle size and size distribution can be reproducibly controlled by the addition volume of the sodium citrate solution. AuNPs of different sizes coated with 2-mercaptopropionic acid (MSA) were synthesized by adding different amounts of the smallest citrate coated AuNPs (16.7 ± 1.7 nm) to a solution containing MSA and HAuCl_4 at a fixed molar ratio under rigorous stirring. The color change of the reaction mixture (pink to purple) reflects the growth of AuNPs. The size of the synthesized AuNPs ranges from 20 nm to 120 nm. Morphological characterization of AuNPs was done with transmission electron microscopy (TEM) and dynamic light scattering (DLS) measurements. All synthesized particles were mono-dispersed and quasi-spherical in shape (Fig. 1).



The synthesis of Nanotags, namely Raman reporter dye encoding of synthesized AuNPs, is achieved using the method described by Qian *et. Al.* A freshly prepared Raman reporter dye solution was added to a mono-dispersed AuNP solution (1.1×10^{10} particles /mL) with the final concentration ranging from 5 μM to 15 μM . The ratio of the dye to AuNPs varies with different dyes. The optimum ratio was determined for each Raman reporter dye that yields the maximum coverage of the dye on the surface of AuNPs without resulting in aggregation. Rate of addition and speed of mixing were also found to be critical in obtaining optimum coverage of dye as reported before. Raman reporter dye coated AuNPs were further pegylated by a mixture of SH-mPEG (10 μM , MW: 5 kDa) and SH-PEG-COOH (1 μM , MW: 2 kDa) solutions at a volumetric ratio of 2:7. The pegylation provides steric stabilization, improved biodistribution properties, and carboxylate groups for further functionalization.

After the dye encoding and pegylation, the resultant Nanotags were again characterized by UV-Vis absorption spectroscopy, TEM, and DLS measurements to ascertain that they were monodispersed and adequately pegylated while retaining their characteristic Raman spectra. A 3-nm red-shift of the plasmon peak of AuNPs was observed as a result from the pegylation. Further a PEG layer was evidently shown on the TEM images (Fig. 1) encapsulating the AuNPs. There was minimal broadening of attenuation curve as measured by the full width at half maximum of the attenuation curve which indicates that the nanotags were not aggregated. In addition, virtually no change in size or size distribution was observed on the DLS histograms. Stability of the nanotags was tested in various solvents (10 mM PBS, 0.1M MES, goat serum, methanol (99.9%), DMSO(99.9%)) at room temperature (Fig. 2). The nanotag solutions were monitored by UV-Vis, DLS, and SERS out to one month with no signs of aggregation or spectral changes, which attested the stability of the nanotags.

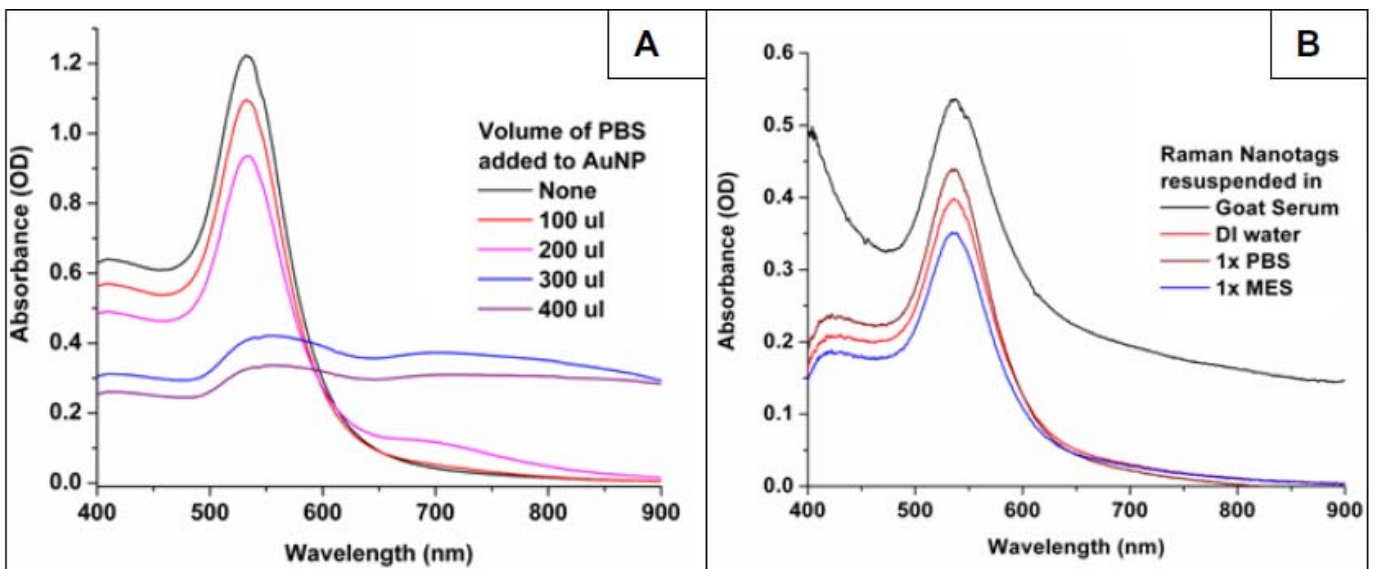


Figure 2: Shows attenuation plots of (A) gold nanoparticles (AuNPs) and (B) nanotags. The attenuation plot of AuNP gradually flattens with increase in volume of 10 mM PBS (1x) however, attenuation curves of the nanotags retain their shape in the different solvents

SERS Characterization: Five different reporter dyes were used to synthesize single-colored nanotags: Cresyl Violet, Rhodamine 6G, Crystal Violet, DTTC and Nile Blue. These dyes are positively charged which readily adsorb to the negatively charged AuNPs. SERS signals from the nanotags were acquired with a home built Raman spectroscopy module. The module is designed to be integrated into the side port of an inverted microscope for simultaneous microscopy and Raman spectroscopy. Input laser is a 785 nm single line laser (Ocean Optics) fiber coupled into the Raman module. All the presented spectra were collected by microscope objective and recorded by a high resolution spectrometer (Ocean Optics, QE65000). The near infrared excitation wavelength was chosen to minimize tissue autofluorescence during in vivo imaging. The incident laser intensity and integration time for all Raman measurements were 10 mW and 8 seconds, respectively. Representative signature Raman spectrum of each color nanotag encoded with a specific Raman reporter dye is shown in Fig. 3.

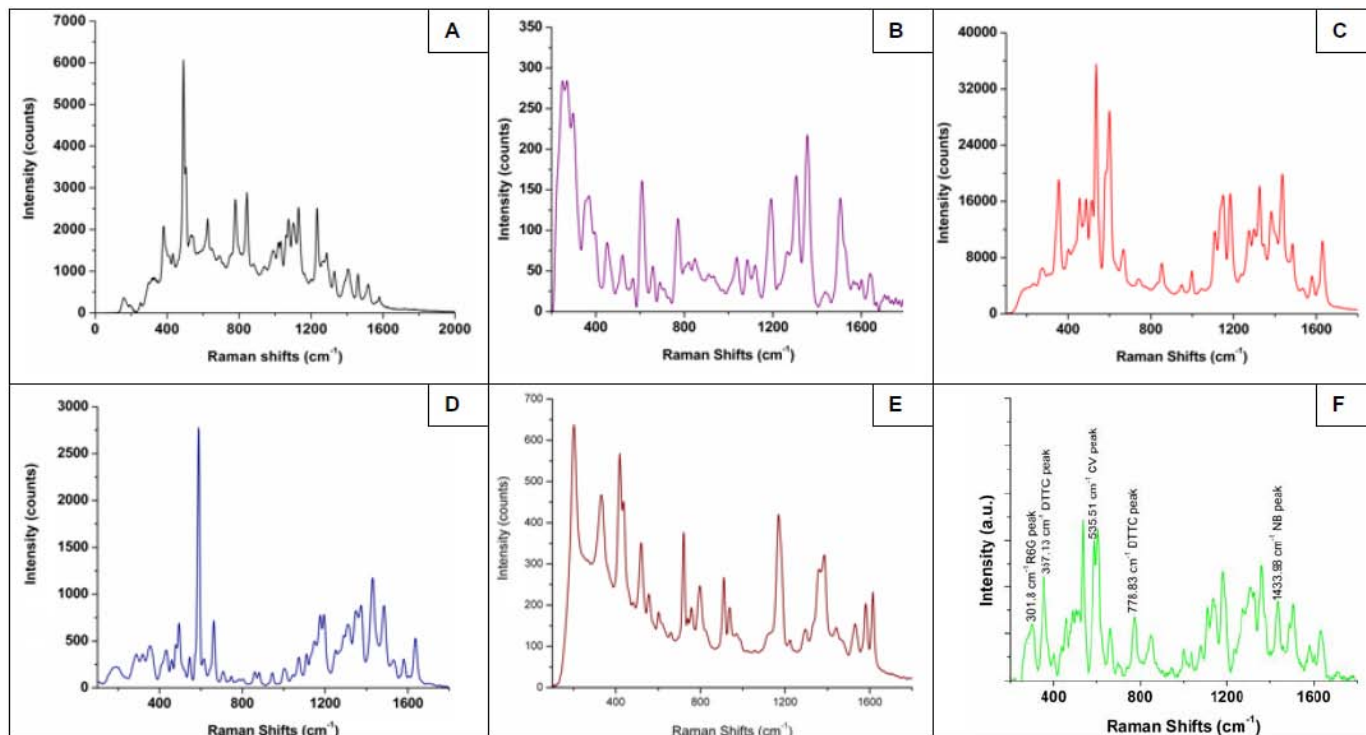


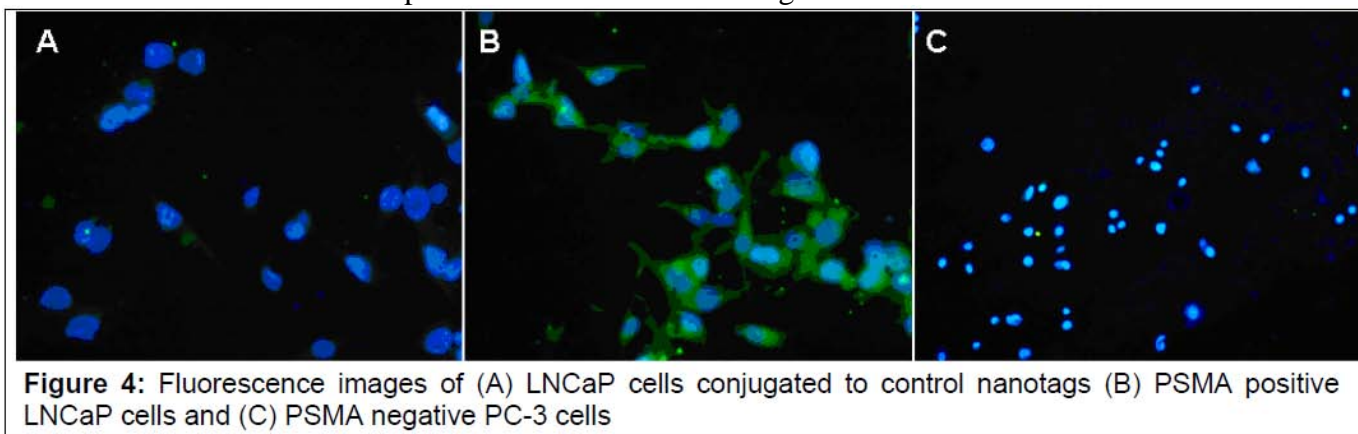
Figure 3: Raman spectra of Raman nanotags with five distinct colors: (A) DTTC iodide (DTTC), (B) Rhodamine 6G (R6G), (C), Cresyl Violet (CV), (D) Nile blue percholate (NB) and (E) Crystal Violet. Each color has a unique spectrum distinguished by the location and magnitude of the various peaks which enable their identification in mixtures. (F) is SERS spectrum of a solution containing a mixture of four color nanotags: Rhodamine 6G, DTTC iodide, Cresyl violet and Nile Blue.

Each color nanotag has a unique spectrum distinguished by the location and magnitude of the various peaks. Although location of some peaks coincide for different nanotags due to a common vibrational mode of specific chemical bonds but there are a number of others peaks which are unique to each reporter dye. Nanotags of different colors show excellent reproducibility of their respective Raman spectrum in terms of the location of the peaks and their relative magnitudes. The absolute magnitude of the Raman spectrum peaks does vary for different batches of synthesized nanotags but consistently a large Raman enhancement is achieved which enables highly sensitive detection of nanotags. The variation in the magnitude of the Raman spectrum is attributed primarily to variation in the amount of dye attached to AuNPs and to a lesser extent variation in the size of AuNPs. Shown in Fig. 3F is the SERS signals measured from a mixture of four single-colored nanotags, specific peaks of a given reporter dye are clearly identifiable in a mixture of nanotags.

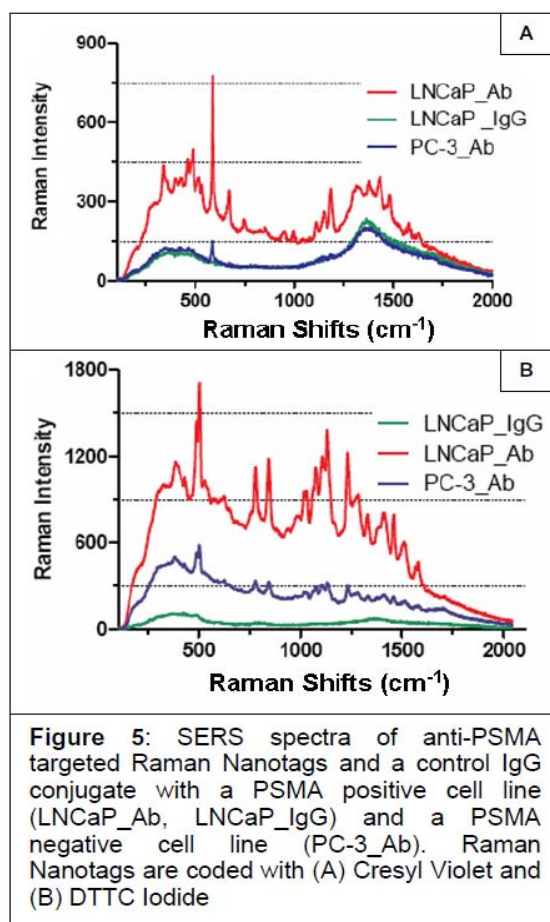
It is noteworthy that the magnitude of Raman peaks shows a linear dependence on the concentration of nanotags. This is critically important for quantitative SERS imaging. The measurement dynamic range of nanotag detection is 30 dB. Nanotags were synthesized from AuNPs with various sizes (20-120 nm) and their Raman spectra were measured. The largest Raman enhancement is obtained for AuNPs with a diameter of 60 – 65 nm. Compared to nanotags synthesized with commercially available spherical shaped AuNPs, the ones built upon our prepared quasi-spherical AuNPs have a larger Raman scattering cross-section as reflected in the Raman spectrum (Fig. 3D). Nanotags colored with DTTC generate the largest SERS signal among the nanotags because the absorption peak (795 nm) of DTTC is very close to the laser excitation (785 nm), which results in resonant SERS.

***In vitro* Cell Culture Studies:** Functionalized nanotags were tested on cells expressing cancer-specific molecular biomarker. Two prostate cell lines (PC3 and LNCaP) were used to demonstrate the specificity of functionalized nanotags binding to cell expressing the cancer specific biomarkers. LNCaP cells express a prostate tumor specific molecular biomarker known as prostate specific membrane antigen (PSMA) where

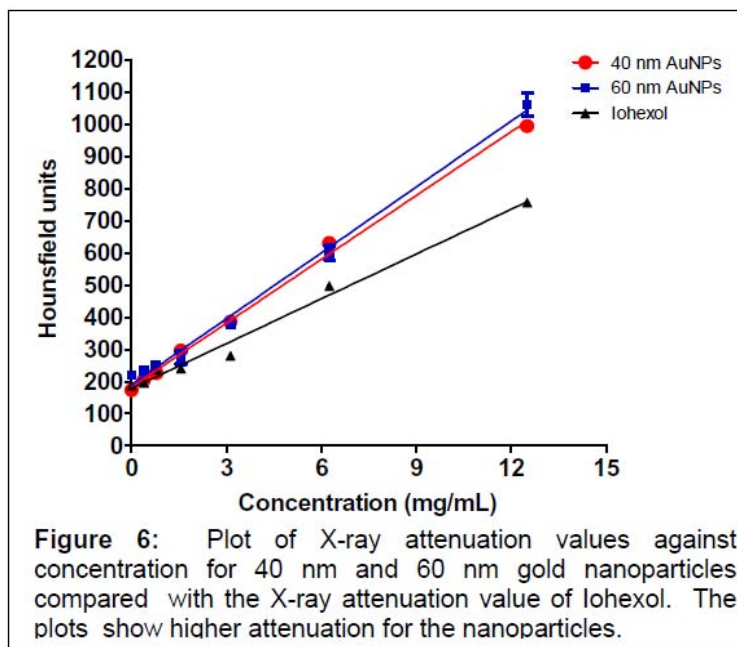
as the PC3 cells do not express it which serves as a control. Nanotags are functionalized by first activating the $-COOH$ groups on the nanotags and then adding anti-PSMA antibodies for bioconjugation to the activated sites. To activate $-COOH$ groups on the surface of nanotags, EDC (*N*-(3-Dimethylaminopropyl)-*N'*-ethylcarbodiimide hydrochloride) and sulfo-NHS (*N*-Hydroxysulfosuccinimide) were added to x ml of nanotags followed by three time centrifugation and resuspension of pellet in PBS for remove of residual EDC and sulfo-NHS. Anti-PSMA and IgG were added to separate solutions of activated nanotags and stored overnight at 4 °C and for bioconjugation. The resulting antibody-nanotag conjugates were purified by either size-exclusion column separation or centricon centrifugation.



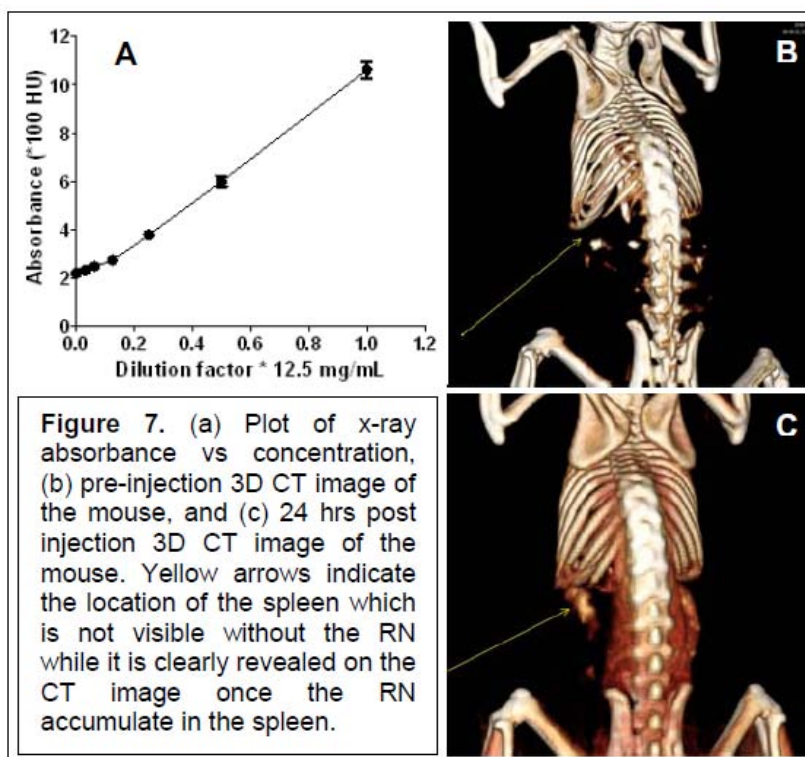
Functionalized nanotags (anti-PSMA and IgG) were incubated in fixed PC3 and LNCap cell in micro volume (100 ul) well and left overnight at 4°C. The cells were gently washed three times with PBS to remove any unbound nanotags. Immunoreactivity of anti-PSMA was confirmed with immunohistochemistry imaging studies. Shown in Fig. 4 are the fluorescence microscopic images of LNCap and PC3 incubated with anti-PSMA antibodies followed by secondary staining with fluorescent antibodies. The LNCap cells clearly show the expression of PSMA (green color) whereas PC-3 cell do not show any expression. The blue color in both the images is the nucleus of the cells visible due to DAPI staining. For SERS imaging the cells were visualized under an inverted DIC microscope with the Raman module is also attached to the inverted microscope. The focus of the excitation beam was positioned on the cell layer to measure the SERS signal. The LNCap cells clearly show the presence of bound nanotags functionalized with anti-PSMA (Fig. 5) on the cells whereas weak or no SERS signal is recorded from nanotags functionalized with IgG. The small SERS signal recorded with nanotags functionalized with IgG is attributed to non-specific binding. No SERS signal attributable to a Raman reported dye (DTTC or CV) is recorded from PC3 cells. The background SERS signal seen is from the glass coverslip.



CT Characterization: X-ray attenuation of the nanotags (60 nm and 40 nm. Size range must be presented) was quantified by a Siemens Inveon PET-CT Multimodality System (Konxville, TN). Vials containing serially diluted nanotags were placed in the CT scanner. The measured X-ray attenuation values of nanotags show a linear dependence on the nanotag concentration (Fig. 9). The offset in the plots is due to the background X-ray attenuation of the plastic vials used to hold the samples. Next, the X-ray attenuation of the nanotags is compared to Iohexol (Omnipaque™, GE Healthcare), an iodine based clinical CT contrast agent. As shown in Fig. 6, both nanotags (60 nm and 40 nm) afforded significantly higher CT contrast than Iohexol at the same concentrations (molar equivalent of gold vs iodine). This clearly indicates the great potential of AuNP-based CT contrast agents to improve the sensitivity of CT. The measured CT contrast of nanotags is 2.67 times higher than that of pegylated 30 nm AuNPs reported by Kim *et. al.*



In vivo CT Contrast of Nanotags: To demonstrate *in vivo* CT contrast of the nanotags, CT images were obtained at 80 kV and 500 mA with a focal spot of 58 μm on the Siemens Inveon PET-CT scanner. The total rotation of the gantry was 360° with 360 rotation steps obtained at an exposure time of approximately 225 ms/frame. Under low magnification the effective pixel size is 103.03 μm . Three Balb/c mice were fasted overnight and scanned under 2% isoflurane anesthesia for the duration of the imaging before receiving 100 μL of 12.5 mg/mL of the 65 nm nanotags via the tail vein. At 24 h post-injection, the mice were sedated and scanned again. Each CT scan time was approximately 6 min. CT images were reconstructed with a down sample factor of 2 using Cobra CT Reconstruction Software.



Reconstructed images were analyzed using the Siemens Inveon Research Workplace (IRW) software. As shown in Fig. 7, the spleen became clearly visible with the AuNP-based nanotags as contrast agent (Fig. 7C). The image quantification revealed that the CT attenuation value was 432 HU in the spleen at 24 h post injection, while it was around 100 HU in other soft tissues. The presence of nanotags in the spleen was

further confirmed by TEM images of the spleen tissue slices. In addition, the TEM images showed that the nanotags were internalized in the spleen cells and preferentially accumulated in the lysosomes. This evidently demonstrates the *in vivo* stability of the AuNP-based nanotags.

***In Vivo* SERS and CT Imaging:** To demonstrate the dual contrasts of SERS and CT of our nanotags *in vivo*, three nude mice were injected with 10 μ L of the 65 nm nanotags at a concentration of 12.5 mg/mL subcutaneously after sedation under 2% isoflurane anesthesia. SERS and CT scans were recorded pre and post injection. The SERS images were recorded followed by CT scanning. For SERS imaging, the sedated mouse was placed on a platform and its body temperature was maintained by a water-circulation heating pad. The SERS spectra were acquired with a $10\times$ (0.25 N.A.) microscope objective with an integration time of 8 sec. Recorded SERS spectra before and after injection of nanotags are shown in Fig. 8A & B, respectively. Representative whole body CT images of the mice before and after the nanotag injection are shown in Fig. 8C & D respectively.

The *in vivo* Raman spectra pre injection are magnified (6 \times) to clearly visualize the Raman peaks of tissue. The *in vivo* Raman spectra of the nanotags remains distinct with little change or distortion in the peaks and their line width. Except for overlapping peaks at 300 and 400 cm^{-1} , the rest can be readily attributed to the reporter dye. Raman spectra of the injected nanotags were also recorded as function of nanotag concentration. Serially diluted solutions of nanotags were injected subcutaneously at various locations. However due to the rapid diffusion of the nanotags in tissue it is difficult to establish the functional

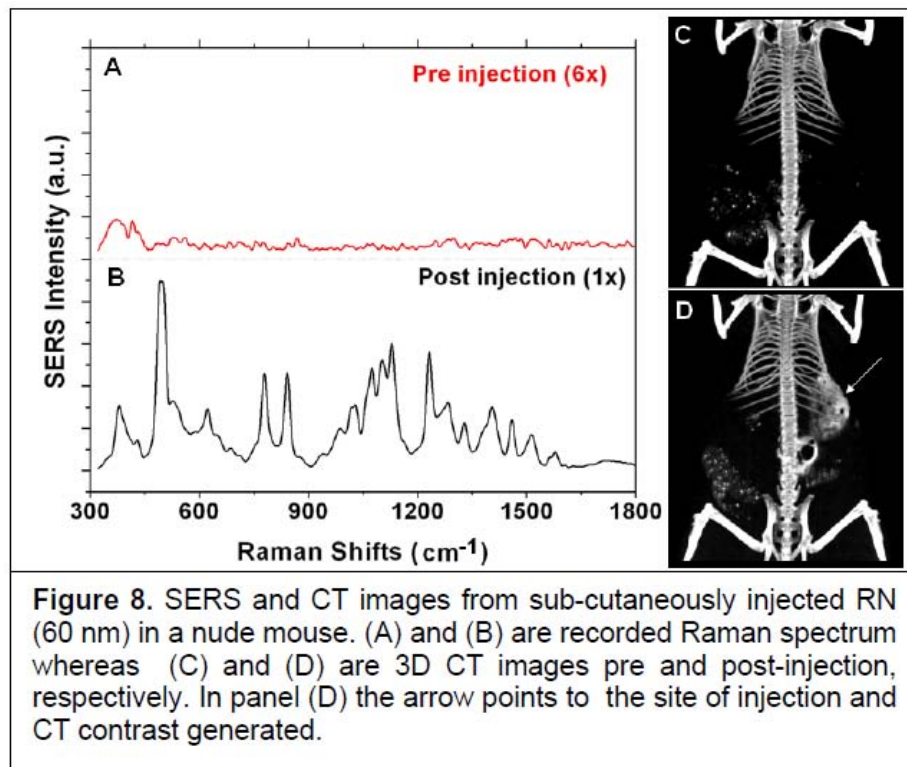


Figure 8. SERS and CT images from sub-cutaneously injected RN (60 nm) in a nude mouse. (A) and (B) are recorded Raman spectrum whereas (C) and (D) are 3D CT images pre and post-injection, respectively. In panel (D) the arrow points to the site of injection and CT contrast generated.

dependence of Raman signal magnitude on the nanotag concentration but nonetheless a robust and distinct Raman spectrum was successfully recorded at the lowest concentration (0.025 mg/mL).

Evaluation of tissue distribution and *in vivo* pharmacokinetics of Raman Nanotags in mice: The importance of the tissue distribution and *in vivo* pharmacokinetics of nanoparticles has been well recognized, however in most of recently published work on biomedical applications of a variety of nanoparticles, it is largely neglected. As for AuNP based nanoparticles, the current biodistribution method is limited to ICP-MS, which is a labor intensive and time consuming process. It is very hard if not impossible to apply the ICP-MS method for systematic *in vivo* evaluation in an efficient manner. To overcome this problem, we have taken advantage of the superior sensitivity of radiotracers by using a gamma emitting gold isotope, ^{198}Au ($t_{1/2} = 2.70$; $\gamma: 0.412$ MeV), to enable efficient gamma counting of tissues of interest. The isotope is weekly produced at the University of Missouri Research Reactor. Given the identical chemical properties of $^{198}\text{AuCl}_3$ and cold AuCl_3 , the synthetic procedures of AuNP based Nanotags are essential the same when a trace amount of $^{198}\text{AuCl}_3$ is used. In addition, the reasonably long (or short) half life of ^{198}Au do not impose any time restraints on any of the above synthetic procedures or

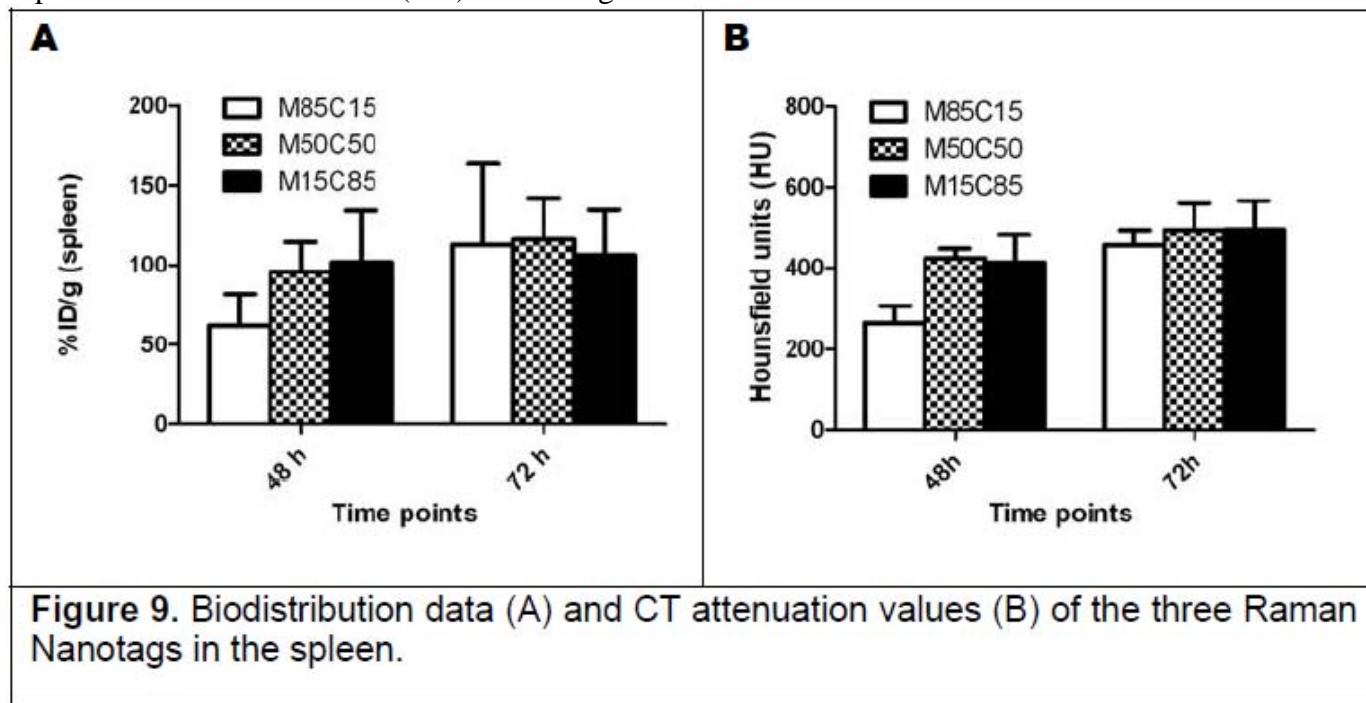
excessive radiation exposure to the chemists. Other radiotracer approaches include labeling the nanoconstructs with gamma or positron emitting isotopes through a covalent attachment of a bifunctional chelator to the nanoparticles surface. However, in addition to the aforementioned advantage, our method is advantageous in two other aspects 1) incorporation of ^{198}Au into the AuNP core offers an intact surface for further modifications if targeting and/or drug loading are needed; and 2) no bifunctional chelators are needed as in conventional radiolabeling of nanoparticles. This avoids the concerns of in vivo transchelation of metal ions from the chelators/nanoparticles, which has been well documented in the literature, and thus ensures the integrity of the multiplexed Raman Nanotags and faithfully reflects their biological behavior in live subject.

To evaluate the surface charge effect on the tissue distribution profiles and PK parameters, $^{198}\text{Au}/\text{AuNP}$ nanoplateforms differing in the molar ratios of HS-PEG-COOH (C) and HS-mPEG (M) were synthesized (C15M85: 15C:85M; C50M50: 50C:50M; C85M15: 85C:15M). The pegylated nanoplateforms can be prepared at a concentration up to 15-mg (Au)/mL. However a rather diluted solution (0.05 mg/mL) was used for the following biodistribution experiments to maintain 5 μCi of ^{198}Au activity per mouse, which is equivalent to 5 μg of Au injected into each animal. All animal studies were performed in compliance with guidelines set by the UT Southwestern Institutional Animal Care and Use Committee. The injected doses were prepared by diluting the purified $^{198}\text{Au}/\text{AuNP}$ nanoplateform with 10 mM PBS buffer. Normal 4 – 5 wk male healthy balb/c mice (Harlan, IN) were anesthetized with isoflurane and then injected with 100 μL of each $^{198}\text{Au}/\text{AuNP}$ nanoplateform (*ca.* 5 $\mu\text{Ci}/\text{mouse}$) via the tail vein. The animals were anesthetized again prior to sacrifice at 24 h, 48 h, and 72 h post-injection (p.i.) ($n = 4$ at each time point). Organs of interest (blood, heart, lung, liver, spleen, kidney, fat, muscle, intestine, stomach, and thyroid) were removed, weighed, and counted. Standards were prepared and counted along with the samples to calculate the percent injected dose per gram tissue (%ID/g) and percent injected dose per organ (%ID/organ). The animals of the last time point groups were housed in metabolic cages (4 mice per cage) to collect urine and feces at 24 h, 48 h, and 72 h p.i. For the evaluation of pharmacokinetic (PK) parameters, 5 – 10 μL of blood was collected from the retroorbital sinus of the animals at 5 min, 10 min, 20 min, 40 min, 1 h, 4 h, and 24 h p.i. The PK parameters were calculated based on a two-compartment open model.

In order to identify optimal AuNP nanoplateforms with desired in vivo properties for the development of Nanotags, systematic biodistribution studies have been done in normal male BALB/c mice since the last submission using $^{198}\text{Au}/\text{AuNP}$ nanoparticles in diameter of 16.7 ± 1.7 nm, 43.9 ± 3.8 nm, and 65.6 ± 6.4 nm. The evaluated variables include: 1) Nanoparticle size (depicted in Fig. 13 as 20 nm, 40 nm, 60 nm, respectively, for simplicity); 2) PEG chain length (2 KDa and 5 KDa); and 3) surface charge (namely, molar ratio of HS-PEG-COOH/HS-mPEG: 15:85; 50:50; and 85:15). Consistent with previous reports, the non-targeted $^{198}\text{Au}/\text{AuNP}$ Raman Nanotags predominately deposited in the liver and the spleen, while their uptake in other organs was negligible. From 48 h to 72 h p.i., the retention of the nanoparticle appears rather steady. Among the $^{198}\text{Au}/\text{AuNP}$ nanoplateforms, M50C50 exhibited the lowest uptake in the liver, while M85C15 showed the lowest accumulation in the spleen at 48 h p.i. Overall the surface charge varied by the molar ratio of HS-PEG-COOH and HS-mPEG didn't significantly alter the biodistribution profiles of the AuNP based Raman Nanotags. Limited by space, biodistribution and in vivo kinetic data are not presented. It should be pointed out that the optimal nanoplateform selection is dependent on the application, for which the nanoplateform is intended. Given the aims of this project, desired properties of AuNP nanoplateforms for further development of Nanotags include: *low uptake in non-target organs (especially liver, spleen, and bone marrow), reasonable long blood circulation time ($t_{1/2\alpha} > 30$ min) so that the nanoplateforms have adequate time to reach the targets before trapped in the RES organs, and strong SERS signal.* After taking these factors into consideration, we have chosen two AuNPs as nanoplateforms to develop Nanotags for future studies: 43.9 ± 3.8 nm and 65.6 ± 6.4 nm AuNPs coated with HS-PEG-COOH/HS-mPEG at a fixed molar ratio of 50:50 (PEG: 5 KDa).

Ex vivo determination of CT attenuation values of Raman Nanotags in the spleen: CT scans were performed on a Siemens Inveon PET-CT Multimodality system (Siemens Medical Solutions Inc.,

Knoxville, TN). The CT Imaging was obtained at 80 kV and 500 A with a focal spot of 58 μm . The total rotation of the gantry was 360° with 360 rotation steps obtained at an exposure time of approximately 225 ms/frame. The images were attained using a CCD readout of 4096 x 3098 with a bin factor of 4 and an average frame of 1. Under low magnification the effective pixel size was 103.03 μm . The total CT scan time was approximately 6 min. CT images were reconstructed with a down sample factor of 2 using Cobra Reconstruction Software. Reconstructed images were analyzed using Inveon Research Workplace (IRW) software. For each organ of interest, five similarly sized regions of interest were placed in the areas expressing the highest contrast as determined by visual inspection. The resulting quantitative data was expressed in Hounsfield Units (HU) and averaged.



Since the spleen showed the highest uptake of $^{198}\text{Au}/\text{AuNP}$ nanoplateforms ($\sim 5\% \text{ID/g}$), we performed ex vivo CT scans of the spleen tissues after biodistribution. As shown in Figure 9, the CT attenuation values (Fig. 9B) of the spleens (whole) correlate well with the uptake values ($\% \text{ID/g}$; Fig. 9A) measured by biodistribution experiments. Notably 5% of the injected dose ($\sim 0.25 \mu\text{g Au}$) resulted in ~ 400 HU in the spleen tissue. If we use a 1 mg (Au)/mL of Rama Nanotag solution to prepare the injection doses, a 1%ID/g uptake value in a tumor with the similar spleen size (50 – 100 mg) would be able to offer a CT attenuation value > 100 HU assuming the biodistribution profile maintains the same. Given that the typical CT attenuation values of soft tissues are in the range of 0 – 50 HU, we anticipate that tumors with $> 1\% \text{ID/g}$ uptake be revealed on CT images.

In Vivo Tumor Imaging Tumor (orthotopic prostate tumor model) bearing mice were injected with Raman Nanotags (RN) and imaging studies were carried out at different time points. Tumor cells (PC-3) cell suspension was injected orthotopically (20k DAB2IP knockout PC-3 cells per injection, injection volume of 100 μL) into the prostates of 5 nude mice. After the injection of cells, the animals were monitored everyday. This orthotopic prostate cancer metastasis animal model was provided by Dr. Jer-Tsong Hsieh's in the Department of Urology at UT Southwestern. The tumor was allowed to grow for 1 week for *in vivo* imaging studies. Five tumor-bearing mice were fasted overnight before injected with 100 μL of 100 μCi of FDG solution. PET/CT scanning was performed at 1 hr p.i. When the orthotopic tumors were clearly denoted by PET imaging, 100 μL concentrated RN ($43.9 \pm 3.8 \text{ nm}$) of 12.5 mg/mL dosage was injected intravenously via the tail vein. CT scans were carried out for 3 days. After mice were sacrificed, organs of interest, such as the spleen, liver and tumors were taken out for SERS and TEM characterization. The TEM images clearly show the uptake of RN in the tumor (Fig. 10A&B).

Corresponding SERS from RN in tumor are shown in Fig. 10C. Overlap of CT (pre and post RN injection) and PET (^{18}F FDG) images of tumor metastasis are shown in Fig. 11. *Clearly the metastasis from the tumors in the prostate was visualized by RN-aided CT. The result was further verified by FDG-PET.*

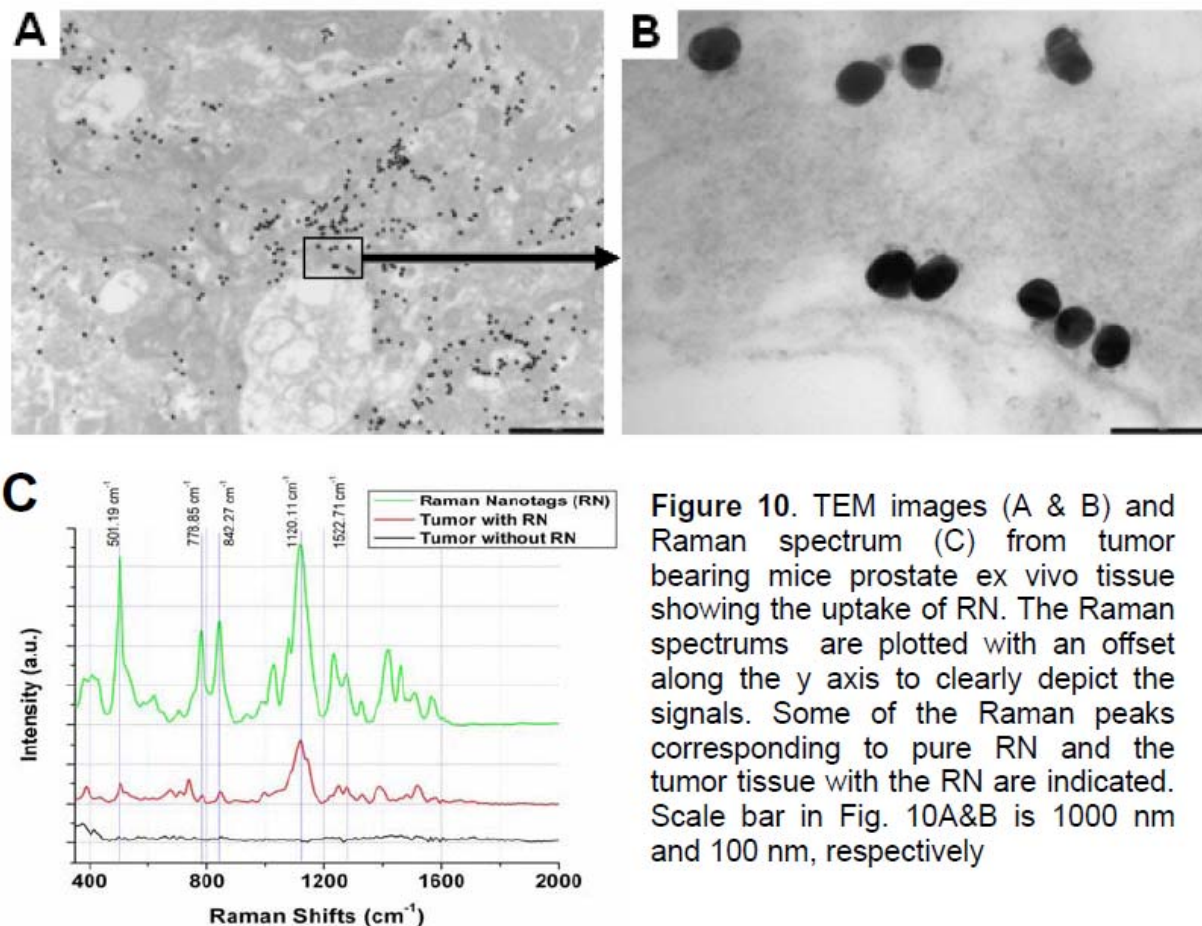


Figure 10. TEM images (A & B) and Raman spectrum (C) from tumor bearing mice prostate ex vivo tissue showing the uptake of RN. The Raman spectrums are plotted with an offset along the y axis to clearly depict the signals. Some of the Raman peaks corresponding to pure RN and the tumor tissue with the RN are indicated. Scale bar in Fig. 10A&B is 1000 nm and 100 nm, respectively

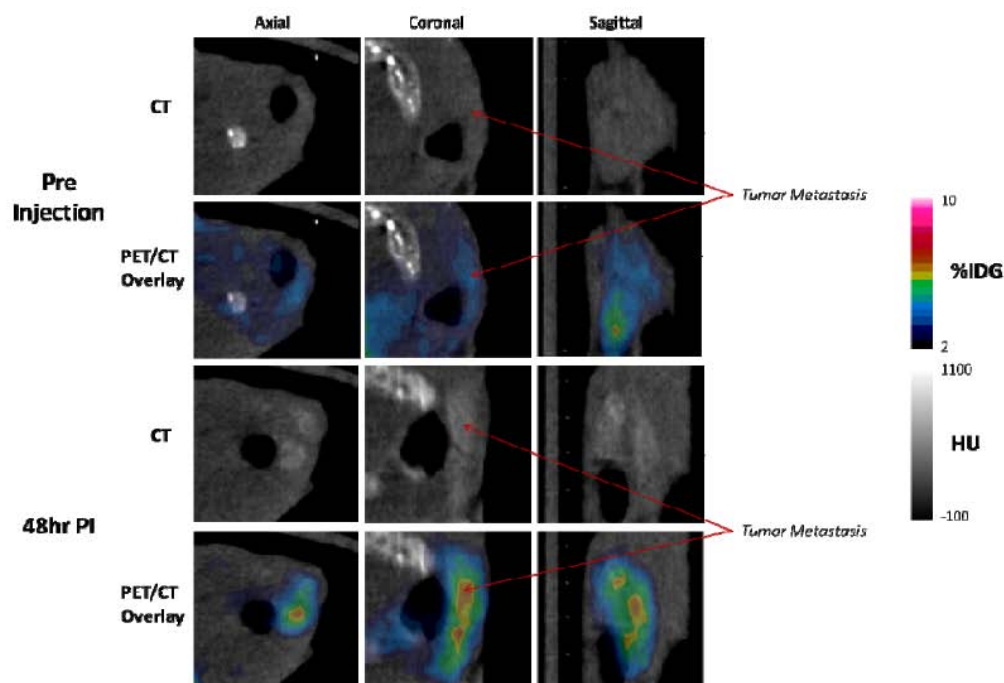


Figure 11. In vivo PET/CT imaging of RN and ^{18}F FDG in nude mice with prostate tumor metastases. Prior to RN injection, control images were taken. CT units are expressed in Hounsfield Units (HU) and PET units are expressed in %ID/g. Tumor metastasis sites are indicated with red arrows on the coronal view of the mouse for both pre and post injection. The images above depict the same slice of the animal pre and post injection.

ii) **Cu-64 incorporated gold nanoparticles as dual modality (PET/CT) imaging agents for prostate cancer detection**

Rationale:

It has been well-recognized that no single modality is perfect or sufficient to afford all desired information. For instance, CT has supremely high resolution but with low sensitivity, while PET is exceptionally sensitive, metabolically functional but with poor spatial resolution. Therefore the synergistic combination of these two imaging techniques will certainly be advantageous over CT or PET alone. Indeed recently we have seen the hybrid PET/CT scanners have completely replaced the standalone PET system in the United States. To enable PET/CT studies of biological events at the molecular or cellular level, novel dual modal imaging agents are highly desirable.

In this project, we applied our developed approach to incorporate ^{64}Cu , a positron emitter, to the same gold nanoparticle platform, whose potential as CT contrast agent has been shown in project i).

Accomplished Work

Synthesis of ^{64}Cu -incorporated AuNP: The AuNPs were synthesized using the procedure as described above. In brief, to prepare citrate coated ^{64}Cu -incorporated AuNPs, an aqueous solution of 0.25 mM HAuCl_4 (50 mL) with $^{64}\text{CuCl}_2$ (8 mCi) was heated to boiling with constant stirring, to which a certain volume of 1% (wt) sodium citrate (0.40 – 1.75 mL) was added. Within a minute, the solution turned from faint blue to red indicating the formation of AuNPs. The boiling and stirring were continued for 30 min. The resulting solution was then cooled down to room temperature, which afforded AuNPs with a mean diameter of ~ 40 nm as determined by TEM.

In Vivo Dual Modality Imaging in a PC-3 tumor bearing mouse model: PC-3 cells were cultured in T-media at 37 °C in an atmosphere of 5% CO_2 and were passaged at 75 % confluence in P150 plates. T-media was supplemented with 5% Fetal Bovine Serum (FBS) and 1 × Penicillin/Streptomycin. Cultured PC-3 cells were harvested from monolayer using PBS and trypsin/EDTA, and suspended in T-media with 5% FBS. The cell suspension was then mixed 1:1 with Matrigel™ and injected subcutaneously (2.5×10^6 cells per injection, injection volume 100 μL) into the nape of neck of nu/nu mice. After the cell injection, the animals were monitored three times a week by general observations. The tumor was noticed to grow in the first week and allowed to grow three weeks to reach 50 – 100 mg for the imaging studies. Small animal PET/CT imaging studies were performed using a Siemens Inveon PET/CT Multimodality System (Knoxville, TN, USA). Three mice were injected with ~120 μCi of ^{64}Cu -incorporated AuNPs via the tail vein. Ten minutes prior to imaging, the animals were anesthetized using 3% Isoflurane at room temperature until stable vitals were established. Once the animal was sedated, the animal was placed onto the imaging bed under 2% Isoflurane anesthesia for the duration of the imaging. The CT data was acquired at 80kV and 500 μA with a focal spot of 58 μm . The total rotation of the gantry was 360° with 360 rotation steps obtained at an exposure time of approximately 200 ms/frame. The images were attained using a CCD readout of 4096 × 3098 with a bin factor of 4 and an average frame of 1. Under low magnification the effective pixel size was 103.03 μm . The total CT acquisition time was approximately 6 min. CT images were reconstructed with a down sample factor of 2 using Cobra Reconstruction Software. The PET imaging acquisition was performed directly following the CT scans at 4 h, 24 h, and 48 h post injection. PET images were reconstructed using Fourier Rebinning and Ordered Subsets Expectation Maximization 2D or 3D (OSEM2D or OSEM3D) algorithm. Reconstructed CT and PET images were fused and analyzed using the Siemens Inveon Research Workplace (IRW) software.

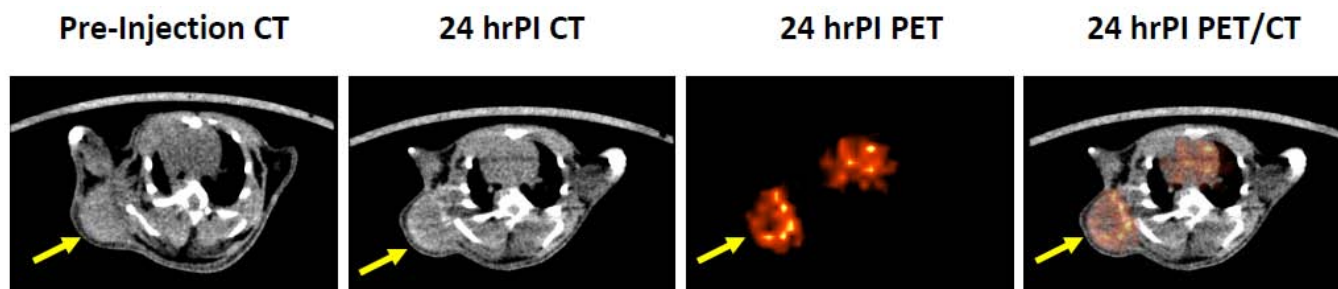
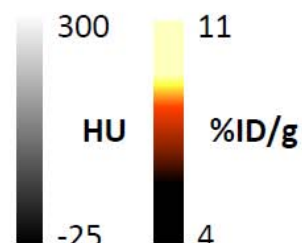


Figure 12. Representative PET/CT imaging of ^{64}Cu -incorporated AuNP. Prior to AuNP injection, control CT images were taken on SCID mice with PC3 cells implanted subcutaneously. The tumors were allowed to grow for 12 days before imaging. Directly after the CT imaging, ^{64}Cu -incorporated AuNP (120 μCi) was injected intravenously into the mice. PET/CT imaging was acquired at 24 hours post injection. CT units are expressed in Hounsfield Units (HU) and PET units are expressed in Percent Injected Dose per Gram (%ID/g). The images above depict the same slice of the animal pre and post injection.



Clearly, the dual modality image nanoprobe revealed a ring shaped signal enhancement, which may reflect the vasculature of the tumor. Notably, this unique tumor vasculature feature was not visible on FDG-PET-CT images.

Construction of PSMA-Targeted Nanoprobes (Objective II)

As shown in the above *In vitro* Cell Culture Studies (Figures 4&5), we have accomplished the construction and *in vitro* evaluations of PSMA-targeted nanoconjugates. However, the nanoplatform that we used was gold nanoparticles instead of iron oxide nanoparticles as proposed in the project due to the availability of As-74. In addition, we were able to obtain a PSMA targeting aptamer from Dr. Ellington's lab at UT Austin to construct another PSMA-targeted nanoconjugate as detailed below.

Construction of PSMA-targeted AuNP-Aptamer conjugates: An aptamer that target PSMA with a common extended GAA UUA AAU GCC CGC CAU GAC CAG was provided by Dr. Andrew Ellington's laboratory. The conjugation of the aptamer to the surface of AuNPs was carried out according to an established procedure from Dr. Ellington's lab that was recently published (1). Briefly, our AuNPs were be firstly coated with an oligonucleotide with a sequence complementary to the extended sequence of the aptamers in the pegylation procedure (2). The oligonucleotide (5'/ThioMC6-D/Sp18/CTG GTC ATG GCG GGC ATT TAA) TTC was purchased from IDT DNA Technologies. The unreacted capture oligonucleotide and other PEG molecules were removed from the oligonucleotide- and PEG-coated gold nanoparticles by centrifugation. The PSMA targeting aptamer was then hybridized to the modified AuNPs by warming the solution at 70 °C for 5 min followed by incubation at room temperature for 30 min. The unreacted aptamer molecules were removed from the aptamer-conjugated AuNPs by centrifugation. The aptamer-AuNP conjugates were characterized by our established HPLC, DLS, and TEM methods. Further studies are ongoing.

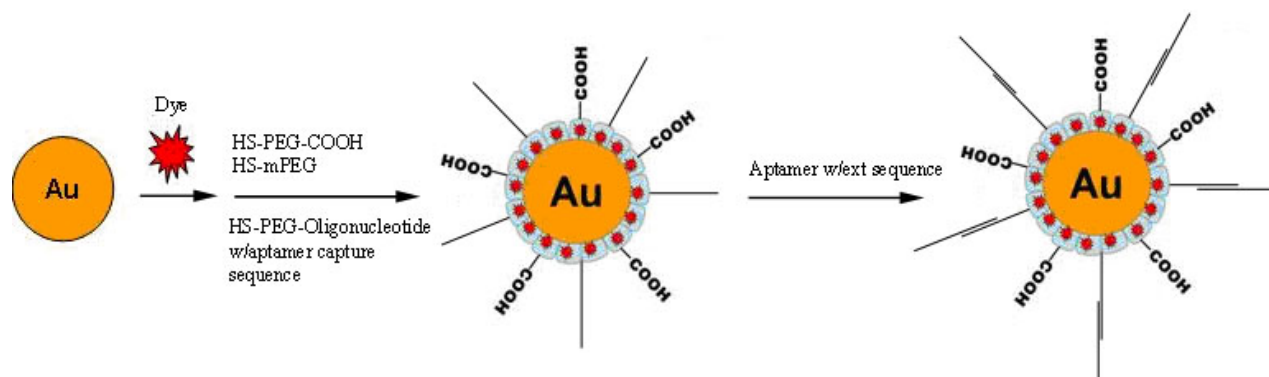


Figure 13. Schematic conjugation of aptamer to the surface of AuNPs.

Key Research Accomplishments

In addition to the accomplishments that were summarized in my 3rd annual report, we have achieved the following ones:

- 1) Successfully constructed two PSMA-targeted nano-conjugates using a monoclonal anti-PSMA antibody and a PSMA-targeting aptamer.
- 2) Successfully applied our developed methodology to a different nanoplatform (AuNP) to develop multimodality imaging probes for prostate cancer detection;
- 3) Successfully visualize prostate cancer metastases on the small intestines in an orthtopic prostate cancer mouse model by CT using AuNP-based Raman Nanotags as contrast agents. The CT result was further confirmed by the clinical gold standard, FDG-PET, ex vivo SERS, and TEM images.
- 4) Successfully incorporated ⁶⁴Cu, a positron emitter, to gold nanoparticles; and performed PET/CT imaging of prostate cancer using the ⁶⁴Cu-incorporated AuNPs.
- 5) PET/CT images enabled by ⁶⁴Cu-incorporated AuNPs showed a unique feature of tumor vasculature in vivo, probably indicating the neovasculature formation.

Reportable Outcomes

One oral presentation by Ms. Yi Guo in the DOD IMPaCT meeting in Atlanta, Georgia, September 5 – 8, 2007

A Master of Science Thesis entitled “DEVELOPMENT OF IRON OXIDE BASED NANOPARTICLES AS DUAL-MODALITY IMAGING PROBES” by Ms. Yi Guo, Graduate Program of Radiological Sciences, Graduate School of Biomedical Sciences, UT Southwestern Medical Center at Dallas. Mentor: Xiankai Sun, PhD

A publication in *Journal of Biomedical Nanotechnology* (a pdf copy is attached):

Zhou Y, Gulaka P, Zhou J, Xiao M, Xu D, Hsieh J-T, Kodibagkar V, and **Sun X**: Preparation and Evaluation of a Radioisotope-incorporated Iron Oxide Core/Au Shell Nanoplatfom for Dual Modality Imaging. *J. Biomed. Nanotechnol.* 2008, 4:474-481

A publication in *Nanotechnology* (a pdf copy is attached)

Xiao M, Nyagilo J, Arora V, Kulkarni P, Xu D, **Sun X**, Davé DP: Gold Nanotags for Combined Multi-Colored Raman Spectroscopy and X-Ray Computed Tomography. *Nanotechnology*, 2010, 21(3): 1-8

Two manuscripts in preparation are to be submitted within six months (We will send them to the USAMRMC once they are accepted for publication).

Conclusions

In addition to the accomplishments detailed in my 1st – 3rd annual report, we developed gold nanoparticle based tags (nanotags) for combined multi-color surface enhanced Raman spectroscopy (SERS) and X-ray computed tomography (CT). The hybrid nanotags are quasi-spherical gold nanoparticles coated with a Raman reporter dye (color) encapsulated by a monolayer of polyethylene glycol (PEG) molecules with carboxylate functional group for bioconjugation with a ligand. Nanotags of five different colors were synthesized for a range of gold nanoparticle sizes and an optimum size has been established to yield the largest SERS signal and X-ray absorption coefficient that is higher than the iodinated compounds currently used in clinic to enhance contrast of CT imaging. Our preliminary in vivo imaging results with nanotags demonstrate the dual modality imaging capability of SERS and CT with a single nanoprobe. Furthermore, we have incorporated a positron emitter to the core of the AuNP-based nanoprobe to enable PET/CT imaging of prostate cancer by a single dose injection. Although the preparation of PSMA-targeted PET/MRI dual modality imaging probes was impeded by the availability of arsenic-74, we were able to take a different route to develop multi-modality imaging agents based on gold nanoparticles. Therefore I believe we have satisfactorily accomplished the goal set for this project.

Personnel supported by this project

Xiankai Sun, PhD, Assistant Professor of Radiology, UT Southwestern
Vikram Kodibagkar, PhD, Assistant Professor of Radiology, UT Southwestern
Padmakar Kulkarni, PhD, Professor of Radiology, UT Southwestern
Yi Guo, MS student of Radiological Sciences, UT Southwestern
Jennifer Stanfield, BS, Research Technician, Urology, UT Southwestern

References

- (1) Javier, D. J., Nitin, N., Levy, M., Ellington, A., and Richards-Kortum, R. (2008) Aptamer-targeted gold nanoparticles as molecular-specific contrast agents for reflectance imaging. *Bioconjug Chem* 19, 1309-12.
- (2) Mirkin, C. A., Letsinger, R. L., Mucic, R. C., and Storhoff, J. J. (1996) A DNA-based method for rationally assembling nanoparticles into macroscopic materials. *Nature* 382, 607-9.

Preparation and Evaluation of a Radioisotope-Incorporated Iron Oxide Core/Au Shell NanoplatforM for Dual Modality Imaging

You-Fu Zhou¹, Praveen Gulaka², Jian Zhou³, Ming Xiao^{1,4}, Dongsheng Xu⁴,
Jer-Tsong Hsieh³, Vikram Kodibagkar¹, and Xiankai Sun^{1,*}

¹Department of Radiology, University of Texas Southwestern Medical Center at Dallas, Texas 75390, USA

²Biomedical Engineering Graduate Program, University of Texas Southwestern Medical Center at Dallas, Texas 75390, USA

³Department of Urology, University of Texas Southwestern Medical Center at Dallas, Texas 75390, USA

⁴State Key Laboratory for Structural Chemistry of Unstable and Stable Species, College of Chemistry and Molecular Engineering, Peking University, Beijing 100871, P. R. China

Magnetic gold-coated iron oxide nanoparticles (Fe@Au NPs) have recently emerged as a new type of iron oxide nanoparticle based magnetic resonance imaging (MRI) contrast agents, in which the gold shell provides a conveniently tunable surface for the presentation of multiple functional molecules. Given the versatility of this nanoplatforM and the intrinsic sensitivity limitation of MRI contrast agents, a new approach was developed in this work to incorporate radioisotopes with suitable half-lives into the iron oxide core of Fe@Au NPs and impart the superior sensitivity of nuclear imaging to the nanoplatforM. The incorporation of ⁶⁷Ga was successfully accomplished by co-precipitation of ⁶⁷Ga³⁺ with Fe³⁺/Fe²⁺ ions at a pH ranging from 4–10. The gold coating procedure was carried out by an iterative hydroxylamine seeding process. Upon the gold deposition, the hydrodynamic radius of the nanoparticles was changed from 23.2 ± 2.2 nm to 31.7 ± 2.3 nm, indicating an 8-nm thickness for the gold shell. The Fe@Au NPs were functionalized by lipoic acid (LA) and further conjugated with a polyarginine cell permeation peptide, NH₂GR11. All the Fe@Au NPs stayed nearly 100% intact in either PBS or rat serum within 72 h. Cell labeling with the LA-modified Fe@Au NPs and NH₂GR11-conjugated Fe@Au NPs was conducted by using a human prostate cancer cell line (PC-3). It was shown that NH₂GR11 was able to increase the nanoparticle loading to PC-3 cells by 2–3 times. Shown in a pilot dual-modality imaging study, the LA-modified Fe@Au NP labeled cells could be visualized by both MRI and autoradiography imaging if the labeled PC-3 cell concentrations were above 1 × 10⁵ cells/mL. The cell permeation peptide, NH₂GR11, could significantly enhance the dual-modality detection sensitivity of the nanoplatforM labeled PC-3 cells.

Keywords: MRI, Nuclear Imaging, Prostate Cancer, Cell Trafficking, Superparamagnetic Iron Oxide Nanoparticles (SPIO), Gold Nanoparticles.

1. INTRODUCTION

The ability to longitudinally monitor cell viability or trafficking *in vivo* in a non-invasive manner is of scientific and clinical significance in the development of new cancer therapies. Due to its high spatial resolution and superior soft tissue contrast, magnetic resonance imaging (MRI) techniques have been increasingly used to image magnetically labeled cells with either gadolinium or iron oxide nanoparticle based agents.^{1–7} With the much larger

magnetic moment surrounding each particle, iron oxide based nanoparticles are capable of providing significantly higher MRI contrast (T_2) than traditional gadolinium-based contrast agents (T_1). However iron oxide based T_2 agents also exhibit the inherent weakness of MRI contrast agents, relatively low sensitivity. Thus various approaches have been reported to combine nuclear imaging or optical imaging techniques with MRI in hope for complementary anatomic, functional, and molecular information.⁸ The combination of MRI and optical imaging is straightforward and has been proven successful in preclinical studies. However, its clinical application is

*Author to whom correspondence should be addressed.

hindered by the shallow tissue penetration depth of visible light.^{9–11} Nuclear imaging techniques, such as positron emission tomography (PET), single photon emission computed tomography (SPECT), have high intrinsic sensitivity without the tissue penetration problem. Therefore the development of dual-modality imaging probes that enable simultaneous MRI and nuclear imaging has drawn considerable interest in the field of molecular imaging.^{12–14} In addition, the recent success of PET-MRI scanners is expected to drive the need for such dual modality imaging probes.^{15, 16}

The preparation of PET/MRI or SPECT/MRI probes can be conveniently realized by attaching bifunctional chelators to the surface of iron oxide nanoparticle for radioisotope labeling.¹⁷ However the *in vivo* stability or integrity of the nanosized conjugates must be seriously considered given the fact that the *in vivo* demetallation of metal complexes is inevitable.¹⁸ Gold-coated iron oxide nanoparticles (Fe@Au NPs) have recently shown potential as MRI contrast agents and the gold shell can serve as a functional moiety for further modifications with varieties of functional molecules. In this work, we hypothesized that the incorporation of metallic radioisotopes with suitable half-lives into the core of Fe@Au NPs would avoid the *in vivo* stability problem and impart the nanoplatform with the superior sensitivity of SPECT or PET.

2. MATERIALS AND METHODS

All chemicals were reagent-grade and used as received. $\text{FeCl}_3 \cdot 6\text{H}_2\text{O}$ (>99.0%), $\text{FeCl}_2 \cdot 4\text{H}_2\text{O}$ (>99.0%), NaOH ($\geq 99.0\%$), KSCN ($\geq 99.0\%$), 4-(2-hydroxyethyl) piperazine-1-ethanesulfonic acid (HEPES), *N*-Ethyl-*N'*-(3-dimethylaminopropyl)carbodiimide hydrochloride (EDC), Hydroxy-2,5-dioxopyrrolidine-3-sulfonic acid sodium salt (sulfo-NHS), and H_2O_2 solution (35 wt% in H_2O) were purchased from Sigma-Aldrich (St. Louis, MO, USA). All aqueous solutions were prepared using Milli-Q water (resistivity: 18.2 $\text{MQ} \cdot \text{cm}$), and degassed by bubbling with N_2 gas for 30 min. Phosphate buffered saline (PBS) solution (0.01 M PO_4^{3-} , 0.138 M NaCl, 0.0027 M KCl, pH 7.4) was prepared by using premade powder (Sigma-Aldrich). Gallium-67 was purchased from MDS Nordion (Vancouver, British Columbia, Canada). Amicon filters with molecular weight cutoff (MWCO) of 30 KDa were purchased from Millipore (Bedford, MA, USA).

The separation and purification of nanoparticles were carried out by centrifugal filtration using the Amicon filters on a HERMLE Z-300K centrifuge (Labnet, Woodbridge, NJ, USA). The nanoparticles were characterized by dynamic light scattering (DLS) on a Wyatt's DynaPro (Santa Barbara, CA, USA), transmission electron microscopy (TEM) on an FEI Tecnai G2 Spirit Biotwin Microscope (Hillsboro, OR, USA), size exclusion high performance liquid chromatography (SEC-HPLC) on a

Waters 600 system (Milford, MA, USA) equipped with three in-line detectors: Waters UV2996 PDA UV detector, Wyatt Mini DAWN light scattering detector, and Shell-USA radio detector. The UV absorbance was acquired on a Milton Roy Spectronic 1201 UV-Vis spectrometer. The addition of NH_4OH or NaOH solution was controlled by a syringe pump (KD Scientific Inc., MA, USA). Radioactivity was counted by a WIZARD2 gamma counter (PerkinElmer, Waltham, MA, USA). Autoradiography was measured on a PerkinElmer Cyclone Plus storage phosphor system with OptiQuant software.

2.1. Preparation of ^{67}Ga -Incorporated Fe@Au NPs

The Fe@Au NPs were prepared by modified literature procedures.^{19, 20} A mixture of $\text{FeCl}_3 \cdot 6\text{H}_2\text{O}$ (0.54 g, 2.0 mmol) and $\text{FeCl}_2 \cdot 4\text{H}_2\text{O}$ (0.20 g, 1.0 mmol) was dissolved in 25 mL of Milli-Q water containing 0.09 mL of concentrated HCl (0.11 mmol). To the solution was added 1–2 mCi of $^{67}\text{GaCl}_3$ ($\sim 10 \mu\text{L}$ in 0.1 N HCl), followed by the addition of 20 mL of 1.5 M NaOH or NH_4OH solution dropwise by a syringe pump at a rate of 40 mL/h under vigorous stirring. A black precipitate was formed immediately. The solution was then neutralized with 0.1 M HNO_3 . The resulted iron oxide nanoparticles were separated by four times of filtration (Amicon 30 KDa filter; 5000 rpm (670 g) \times 30 min), twice with 10 mL Milli-Q water and twice with 10 mL of 0.1 M tetramethylammonium hydroxide solution (TMAOH). The nanoparticles were resuspended in 25 mL of the TMAOH solution, of which 0.75 mL was taken out and diluted to 28 mL with Milli-Q water. To the diluted nanoparticle solution was then added 0.75 mL of a solution containing 0.1 M sodium citrate, 0.2 M $\text{NH}_2\text{OH} \cdot \text{HCl}$, and 1% HAuCl_4 . The color of the solution turned from brown (iron seeds) to light red as the gold shell was forming. The process was monitored using UV-vis spectroscopy and DLS.

2.2. Surface Modifications of the Fe@Au Nanoparticles

As shown in Figure 1, the conjugation of Fe@Au NPs (^{67}Ga - or non- ^{67}Ga -incorporated) with $\text{NH}_2\text{GR11}$ was carried out by a two-step procedure. In the first step, lipoic acid (LA), which is a bifunctional linker with both carboxylate and thiol functionalities, was mixed with the diluted Fe@Au NPs to reach a final concentration of 1 mM. During this step, the thiol group of the linker was bound to the gold surface via the gold-thiol interaction, and the carboxylate groups were left intact. Centrifuge filtration was used to remove the excess linker (Amicon 30 KDa, three times of 5,000 rpm for 30 min). In the second step, the solution of LA-modified Fe@Au NPs was mixed with an EDC/sulfo-NHS solution (6.0 mg sulfo-NHS and 4.0 mg EDC in 50 μL of H_2O) and the pH was adjusted to 7–7.5 by adding 1 N NaOH. The

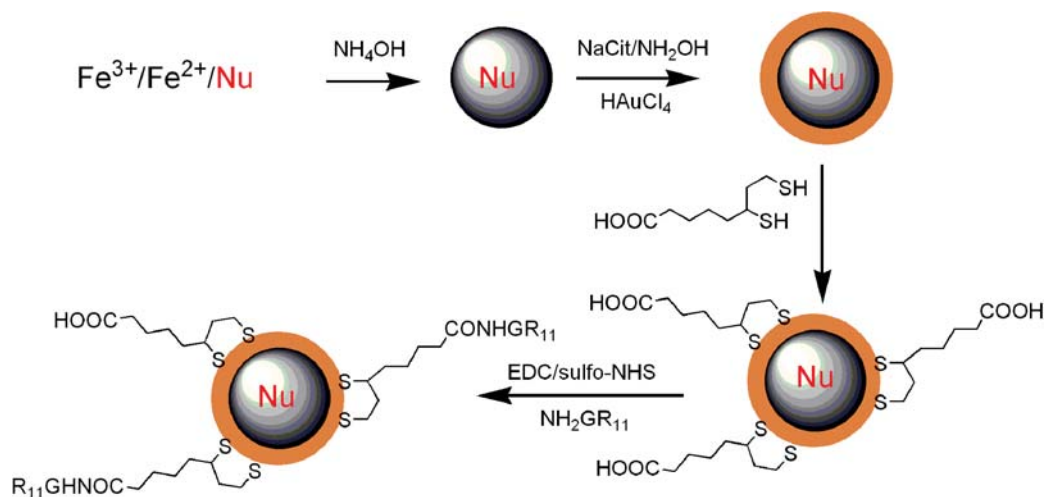


Fig. 1. Schematic synthesis of LA-modified Fe@Au NPs and $\text{NH}_2\text{GR}_{11}$ -conjugated Fe@Au NPs. Nu: Gamma or positron emitting radioisotopes.

resulting mixture was agitated for 30 min at room temperature for the NHS-activated ester formation. Then 10 μL of 10 mg/mL of $\text{NH}_2\text{GR}_{11}$ in DMSO solution was added and mixed thoroughly for 60 min at room temperature. The obtained $\text{NH}_2\text{GR}_{11}$ -conjugated Fe@Au NPs were washed twice with 5 mL of PBS (5,000 rpm for 30 min) and then resuspended in 1.0 mL of PBS solution for further studies.

2.3. Characterization of Fe@Au NPs

The hydrodynamic radii of Fe@Au NPs (^{67}Ga - or non- ^{67}Ga -incorporated) were determined by a Wyatt's DynaPro equipped with a He-Ne laser ($\lambda = 632.8$ nm). Briefly, about 80 μL of Fe@Au NP solution was placed in a quartz microcurvette for the DLS analysis. The scattering data were recorded by appropriate laser intensity (about 500 K counts per second).

The morphology of the Fe@Au NPs was examined by the FEI Tecnai G2 Spirit Biotwin Microscope. The TEM samples were prepared by spreading a drop of the diluted NP solution (0.8 μL) on a discharged copper grid (300 mesh copper Formvar/Carbon).

The iron content of the Fe@Au NPs was measured by a photometric method. In order to calibrate the analysis, a series of standard FeCl_3 solutions (ranging from 0.05 to 0.60 mM, in 2 N HCl) were prepared. To 500 μL of each standard Fe^{3+} solution, 100 μL of 0.1 M H_2O_2 and 400 μL of 0.26 M KSCN were added. The colorimetric reaction was allowed to proceed for more than 1 h before the absorbance was measured at 480 nm. A standard curve ($y = 3.045x - 0.003$) was generated with the linear correlation of 0.999.

2.4. SEC-HPLC Analysis

The quality of Fe@Au NPs was assessed by a SEC-HPLC method using a Waters Ultrahydrogel SEC column (range: 0.5–8000 KDa, 7.8×300 mm) and a Biosuite SEC guard

column (7.5×75 mm). Briefly, 20 μL of Fe@Au NP solution was injected into the SEC column, which was eluted with 20 mM HEPES and 150 mM NaCl buffer at an isocratic flow rate of 1.0 mL/min. Spectra data were collected and processed using the Waters Empower Chromatography Data Software.

2.5. In Vitro Stability of Fe@Au NPs

The *in vitro* serum stability was conducted by adding 20 μL of purified Fe@Au NP samples (^{67}Ga - or non- ^{67}Ga -incorporated) to 180 μL rat serum or PBS. The solutions were incubated at 37 $^\circ\text{C}$ and analyzed by DLS or SEC-HPLC at specific time points.

2.6. Labeling PC-3 Cells with Fe@Au NPs

The PC-3 cell line was obtained from the American Type Culture Collection (ATCC, Manassas, VA). PC-3 cells were cultured in T-medium (Invitrogen Corporation, Grand Island, NY) at 37 $^\circ\text{C}$ with 5% CO_2 and were passed when cells reached 75% of confluency in P100 plates. T-Medium was supplemented with 5% Fetal Bovine Serum (FBS) (Gemini Bio-Products, Woodland, CA) and 1 \times Penicillin/Streptomycin (Sigma, St. Louis, MO). Approximately 1×10^7 cells were mixed with LA-modified or $\text{NH}_2\text{GR}_{11}$ -conjugated Fe@Au NPs (^{67}Ga -incorporated: ~ 2.1 μCi each in 1-mL) in PBS solution and allowed to interact for 5 h in an incubator (37 $^\circ\text{C}$, 5% CO_2). After labeling, the cells were washed by three times of 9 mL PBS solution to remove unbound particles. Then the resulting cells were scratched from the dish and suspended in 5 mL PBS solution, and further washed twice with 5 mL of PBS solution. The Fe@Au NP labeled cells were finally reconstituted with un-labeled cells to 1 mL for either autoradiography imaging or mixed with agarose solution (v/v: 1:2) in order to prevent the cell precipitation during MRI evaluation.

2.7. Determination of Magnetic Relaxivities and MR Imaging

The magnetic relaxivities of Fe@Au NPs were measured in a MR relaxometer (MARAN Ultra, Oxford Instruments) at 23.4 MHz ^1H resonance frequency. MRI measurements of relaxation rates R_1 ($=1/T_1$) and R_2 ($=1/T_2$) were performed on a 4.7 T Varian MRI system (200 MHz for ^1H). A 1% agarose solution in PBS was used to prepare PC-3 cell samples for the MRI studies. Labeled and un-labeled PC-3 cells at various concentrations were homogeneously dispersed in warm ($\sim 40^\circ\text{C}$) agarose phantoms and cooled to room temperature. Each phantom had same concentration of agarose and same total volume (250 μL). These phantoms were placed in a home built solenoid volume-coil and T_1 and T_2 maps were acquired. Four different cell concentrations (1×10^6 , 5×10^6 , 2.5×10^6 , and 1×10^5 cells/mL) of LA-modified Fe@Au NP labeled PC-3 cells or $\text{NH}_2\text{GR11}$ -conjugated Fe@Au NP labeled PC-3 cells were imaged. Two control samples, one with unlabeled PC-3 cells (1×10^6 cells/mL) and the other with no cells (agar only) were also imaged. For the T_1 and T_2 measurements, a 2D spin-echo sequence was employed with varying echo times (TE) and recovery times (TR) on a coronal slice of 1 mm thickness. Maps of the relaxation times T_1 and T_2 were computed on a voxel-by-voxel basis from least-squares fitting of the exponentially varying signals using the analysis routines available on the Varian MR system. Regions of interest (ROIs) were drawn on the maps around each vial to obtain the mean relaxation times T_1 and $T_2 \pm \text{SD}$ and these were converted to relaxation rates R_1 and R_2 , respectively.

2.8. Autoradiography

Autoradiography was measured on a PerkinElmer Cyclone plus storage phosphor system with OptiQuant software. A series of dilutions of PC-3 cells labeled with ^{67}Ga incorporated Fe@Au NPs (LA-modified or $\text{NH}_2\text{GR11}$ -conjugated) were loaded to a 24-well plate. The final volume of each well was 0.75 mL by addition of PBS buffer. A well containing unlabeled 5×10^5 PC-3 cells in 0.75 mL of PBS solution was used as control. The loaded 24-well plate was attached to a phosphor plate with the exposure time of 1 h.

3. RESULTS

As shown in Figure 1, the incorporation of ^{67}Ga into the core of Fe@Au NPs was successfully accomplished. The radiochemical incorporation rate was $39 \pm 3\%$ if 1.5 M NaOH was used in the preparation. In order to improve the incorporation rate, a weak base NH_4OH solution was employed to co-precipitate $^{67}\text{Ga}^{3+}$ and $\text{Fe}^{3+}/\text{Fe}^{2+}$ ions. Under our optimized conditions, a rate up to 83% could be achieved. This is likely because the $\text{Ga}(\text{OH})_3$ compound is

soluble in highly acidic and basic solutions at room temperature. The optimal pH range for the co-precipitation of Ga^{3+} was found to be 4–10.

Gallium-67 incorporated iron oxide seeds were mixed with citrate, and then aliquots of hydroxylamine and HAuCl_4 . Gallium-67 ($t_{1/2} = 3.26$ d) decays by electron capture (EC) and emits gamma rays at various energies (300 KeV: 17%; 185 KeV: 20%; 93.3 KeV: 37%; etc.). Due to the radiation exposure and the isotope's physical decay, the preparation time must be minimized. Therefore we employed centrifugal filters (MWCO 30 KDa) to separate Fe@Au NPs from small species and non-reacted reagents. Because the gold deposition increased the density of the nanoplatform, the magnetic Fe@Au NPs could be separated from the excess iron oxide cores using centrifuge. This expedited separation procedure makes it feasible to prepare such radioisotope-incorporated nanoparticles, especially for the isotopes with short half-lives.

The gold-coating procedure was monitored by the hydrodynamic radius increases (from 23 nm to 29 nm) resulted from the gold deposition as shown in Figures 2 and 3. The UV-vis peak at 520 nm, which is the characteristic surface plasmon (SP) absorption of gold nanoparticles,¹⁹ can also be used to verify the gold shell formation. After the gold-coating, the intensity of the SP peak was increased from 0.72 ± 0.03 to 1.69 ± 0.10 .

After the purification, the ^{67}Ga -incorporated iron oxide NPs and ^{67}Ga -incorporated Fe@Au NPs were

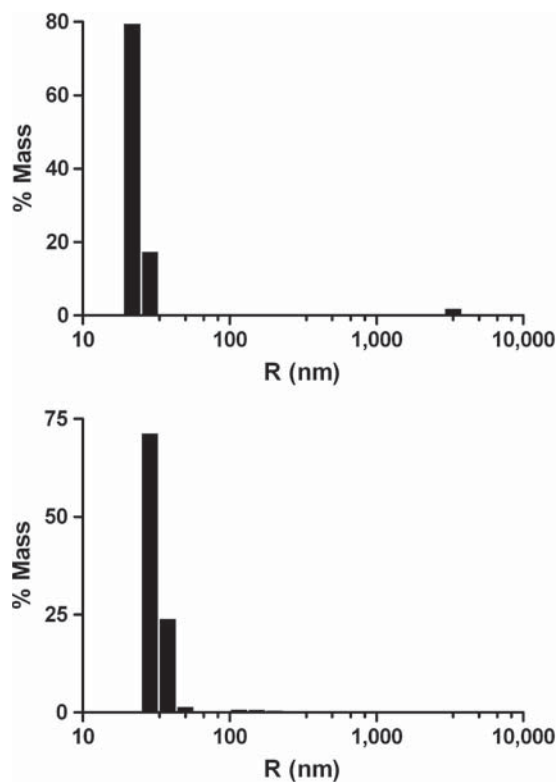


Fig. 2. Changes in hydrodynamic radius of Fe@Au NPs during the formation of Au shell.

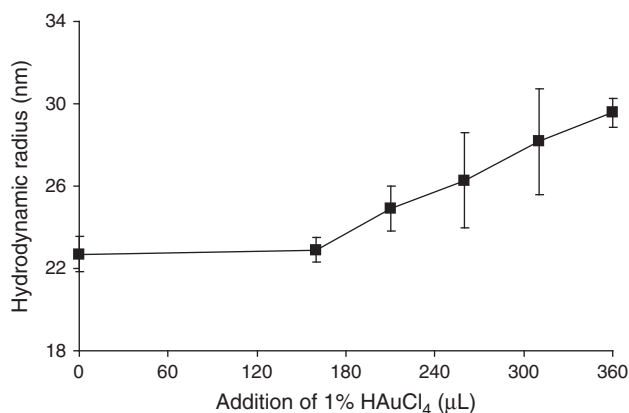


Fig. 3. DLS histograms of the iron oxide core NPs before (upper) and after the gold coating (lower).

characterized by DLS (Fig. 2). Their hydrodynamic radii were 23.2 ± 2.2 nm and 31.7 ± 2.3 nm, respectively, indicating that the gold shell thickness was about 8 nm. The nanoparticles before and after the gold coating show a single peak in their corresponding SEC-HPLC spectra with retention times of 6.7 min and 7.0 min, respectively, indicating a narrow size distribution (from the light scattering detector) and high radiochemical purity (from the radiodetector).

The gold-coated iron oxide nanoparticles were then functionalized by lipoic acid (Fig. 1), which is a bifunctional linker with two free thiol groups at one end and a carboxylate group at the other end. The thiol-Au interaction resulted in the intensity decrease of the SP peak at 520 nm to a constant value (Fig. 4) within 60 min upon the reaction completion of lipoic acid with the gold surface of the iron oxide nanoparticles. The LA-modified Fe@Au NPs (^{67}Ga - or non- ^{67}Ga -incorporated) with carboxylate groups were further functionalized with a cell permeation peptide, $\text{NH}_2\text{GR11}$, which has shown a high affinity to prostate cancer cells,²¹ after being activated with EDC/sulfo-NHS (Fig. 1). The $\text{NH}_2\text{GR11}$ conjugation

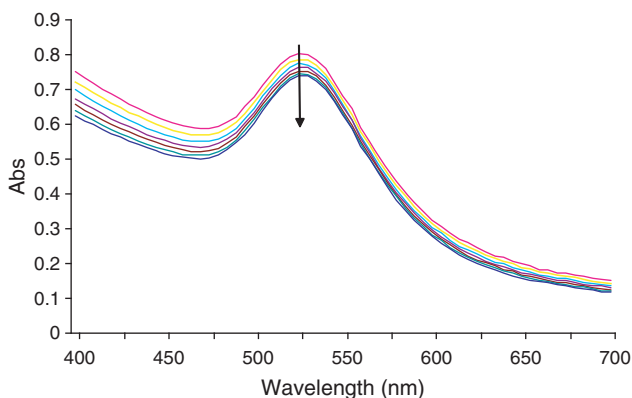


Fig. 4. The characteristic surface plasmon (SP) absorption changes of the Fe@Au NPs during the surface modification of lipoic acid (interval: 5 min).

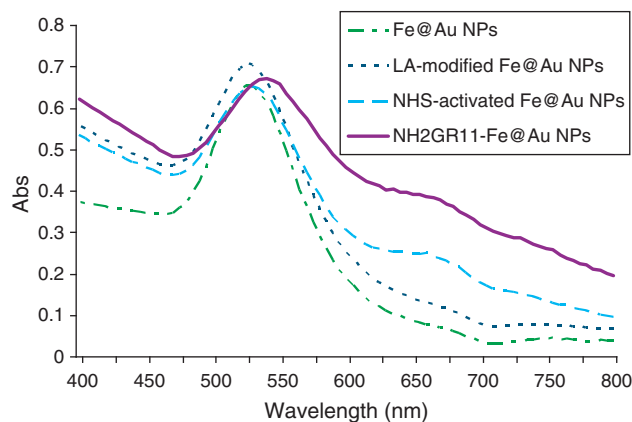


Fig. 5. Comparative UV-vis spectra of Fe@Au NPs, NHS-activated Fe@Au NPs, LA-modified Fe@Au NPs, and $\text{NH}_2\text{GR11}$ -conjugated Fe@Au NPs.

resulted in a 6-nm shift of the SP absorbance spectra (Fig. 5), indicating the formation of the $\text{NH}_2\text{GR11}$ conjugated Fe@Au NPs (^{67}Ga - or non- ^{67}Ga -incorporated). As shown in Figure 6, the sizes of LA-modified Fe@Au NPs and $\text{NH}_2\text{GR11}$ -conjugated Fe@Au NPs were 27.3 ± 6.8 nm. The $\text{NH}_2\text{GR11}$ conjugation did not alter the particle size or size distribution significantly.

The *in vitro* serum stability was evaluated by DLS or SEC-HPLC. All the Fe@Au NP samples stayed nearly 100% intact in either PBS or rat serum within 72 h. Neither aggregation nor decomposition was found.

To label PC-3 cells with the nanoparticle, the cells were first mixed with Fe@Au NPs at 37 °C in an incubator. After a 4-h incubation period and the removal of unbound particles, the iron concentrations were determined by the photometry assay. The iron contents of LA-modified Fe@Au NPs and $\text{NH}_2\text{GR11}$ conjugated Fe@Au NPs in the labeled PC-3 cells were 0.42 mM and 1.23 mM, respectively. This shows that the labeling efficiency of PC-3 cells with the Fe@Au NPs was significantly improved by $\text{NH}_2\text{GR11}$.

LA-modified Fe@Au NPs show a slightly higher translational relaxivity r_2 than the $\text{NH}_2\text{GR11}$ -conjugated Fe@Au NPs (75.6 ± 3.5 $\text{mM}^{-1}\text{s}^{-1}$ versus 64.2 ± 7.4 $\text{mM}^{-1}\text{s}^{-1}$) at 23.4 MHz. This is probably because the modification of $\text{NH}_2\text{GR11}$ resulted in less proton exchanges between the iron oxide core and the surrounding water.

The sensitivity of the dual-modality imaging capabilities of ^{67}Ga -incorporated Fe@Au NPs was assessed by a pilot imaging study. Both LA-modified and $\text{NH}_2\text{GR11}$ -conjugated Fe@Au NPs incorporated with ^{67}Ga were used to label PC-3 cells. A series of labeled cell dilutions were prepared by diluting with non-labeled cells thus maintaining the total cell number the same in each well for autoradiography imaging. As shown clearly in Figure 7, 1×10^4 $\text{NH}_2\text{GR11}$ -conjugated Fe@Au NP labeled cells or 5×10^4 LA-modified Fe@Au NP labeled cells were

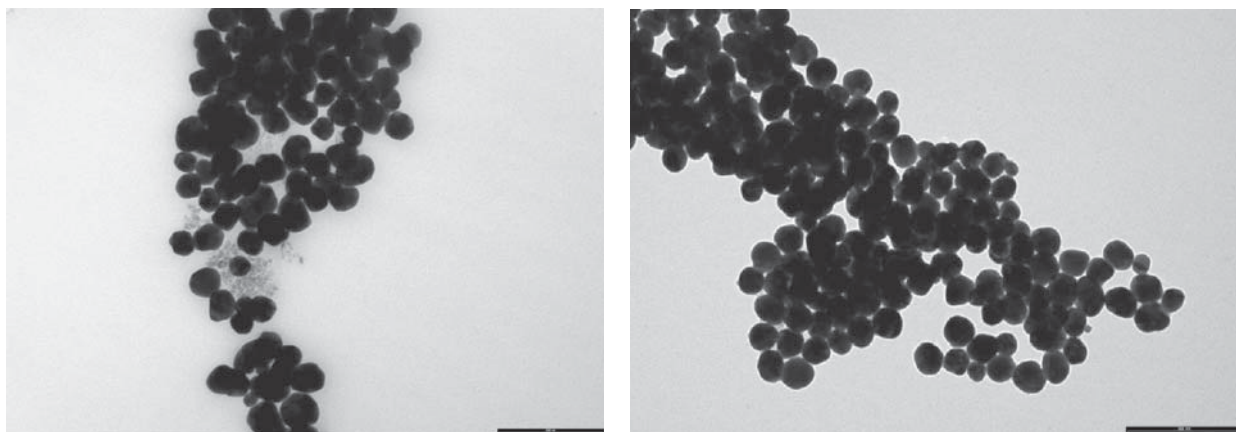


Fig. 6. TEM micrographs of LA-modified Fe@Au NPs (left) and NH₂GR11-conjugated Fe@Au NPs (right). The inset scale bar is 200 nm.

clearly visualized by autoradiography imaging. In the MR studies, at least 1×10^5 LA-modified Fe@Au NP labeled cells (Fig. 8) were needed to show an appreciable increase of R_2 relaxation rate. As shown in Figure 9, the NH₂GR11-conjugated Fe@Au NP labeled cells exhibited

approximately 2–3 times higher of R_2 relaxation rates than the corresponding LA-modified Fe@Au NP labeled cells as well as the controls (Figs. 8 and 9, Table I).

4. DISCUSSION

Nano-architectures have long been explored as carriers for the delivery of therapeutic and diagnostic agents.^{22–25} Of the current nanoplatforms, nanosized superparamagnetic iron oxide (SPIO) holds great promise as MRI probes for non-invasive early detection of signatures of diseases, especially cancer.^{26–31} Indeed the SPIO has been successfully used for MRI imaging of clinically occult lymph-node metastases of prostate cancer.^{32,33} Nevertheless, its sensitivity was substantially lower for the detection of small nodes (<5 mm).^{32,33} Because each imaging modality has its own inherent limitations, developing new probes that can be used in multiple imaging modalities is highly

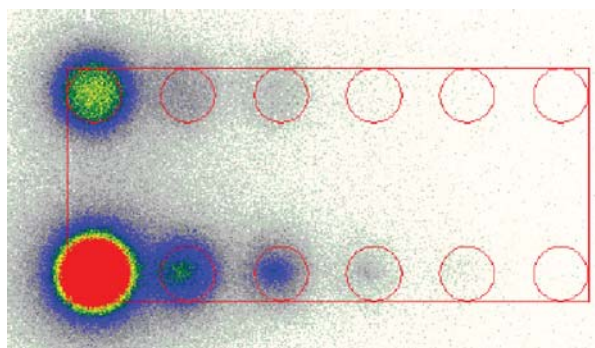


Fig. 7. Determination of the imaging sensitivity of ⁶⁷Ga-incorporated Fe@Au NP using LA-modified or NH₂GR11-conjugated Fe@Au NP labeled PC-3 cells. Autoradiography images of LA-modified Fe@Au NP labeled PC-3 cells (upper row) and NH₂GR11-conjugated Fe@Au NP labeled PC-3 cells (lower row) at concentrations of 5×10^5 , 1×10^5 , 5×10^4 , 1×10^4 , and 5×10^3 cells/mL (from the left to right; the right-most: un-labeled PC-3 cells).

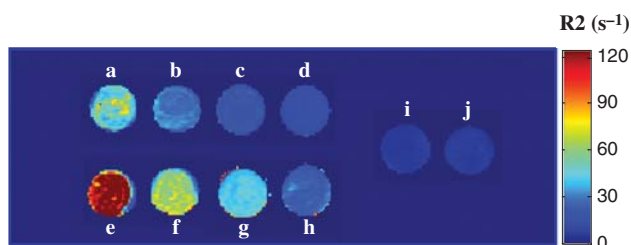


Fig. 8. Comparison of MR imaging sensitivity of LA-modified Fe@Au NP or NH₂GR11-conjugated Fe@Au NP labeled PC-3 cells. R_2 maps of (a–d) LA-modified Fe@Au NP labeled PC-3 cells and (e–h) NH₂GR11-conjugated Fe@Au NP labeled PC-3 cells dispersed in agar phantoms. The concentrations are: (a, e) 1×10^6 , (b, f) 5×10^5 , (c, g) 2.5×10^5 , (d, h) 1×10^5 cells/mL. Also included are control samples with (i) agar (no cells) and (j) 1×10^6 un-labeled PC-3 cells.

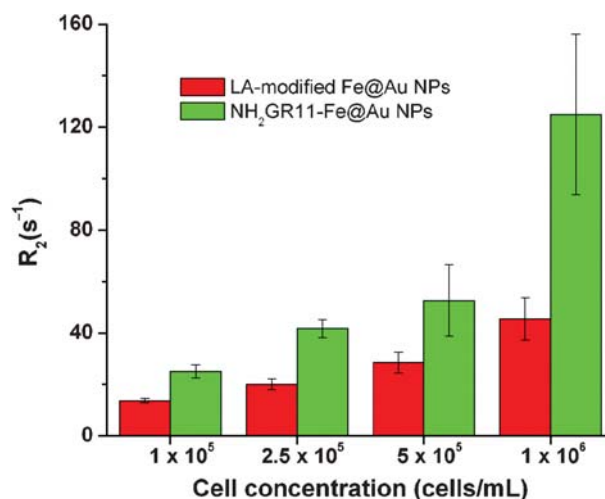


Fig. 9. Effect of NH₂GR11 conjugation on MR imaging sensitivity of labeled PC-3 cells. Bar-graph of R_2 versus cell concentrations of LA-modified Fe@Au NP or NH₂GR11-conjugated Fe@Au NP labeled PC-3 cells.

Table I. Compilation of literature data on cellular uptake of nanoparticles.

Material	Core/core-shell diam. (nm)	Incubation conditions	Stated maximum loading ^a	Corresponding vol. fraction, core only (%)	Method	Refs.
Feridex/TAs	4.8–5.6/ 80–150	2 h 37 °C, 25 μg/ml Fe	30	1.6	Ferrozine/MR	[14]
MION/small molecule	3/38	4 h 37 °C, 0.1 mg/ml Fe	2.2	0.12	FITC immunoassay	[15]
¹¹¹ In-labeled CLIO/Tat peptide	5/45	1 h 37 °C, 40 μg/ml Fe	30	1.6	Gamma counter	[13]
Magnetite (Fe ₃ O ₄)/LHRH	10/?	1 h 37 °C, 7.6 mg/ml Fe	453	23.5	Prussian blue	[18]
Magnetite (Fe ₃ O ₄)/LHRH metastatic tumors	10/?	Tail vein inj, 250 mg/kg NPs, 20 h	78 ± 24	4	Prussian blue (luciferase for metastatic cells)	[18]
Magnetite (Fe ₃ O ₄)/PEG (MW 5000)	10/~60	4 days 37 °C, 0.2 mg/ml NPs	113	5.9	ICP	[16]
Magnetite/PEG-folic acid	44/~94	48 h, 37 °C, unknown conc.	730	37.9	ICP	[17]
Au/citric acid	50	6 h 37 °C, 0.02 nM NPs	9000 NPs/cell	0.11	ICP-AES, UV-Vis	[19]
Au/folic acid-PEG (MW 1500)	10/~30	2 h 37 °C, ~5 × 10 ¹¹ NPs/ml	10 ¹⁵ NPs/mL cell vol.	0.05	TEM on cryoslices	[32]

In converting between mass of Fe and volume fraction, we use the published density for bulk iron oxide, and assume a chemical formula of Fe₂O₃ except where noted. Using the formula Fe₃O₄ does not make a significant difference (~1%). For the gold nanoparticles, we also assume that the density of the nanoparticle cores is the same as that of bulk gold.

^aFor iron nanoparticles, loading is given in units of pg iron per cell.

desirable and attractive. Nanoscaffolds become ideal candidates because multi-presentation of various functionalities can be conveniently made possible on a common platform.

In this study, we developed a new approach to prepare a radioisotope-incorporated iron oxide core/Au shell nanoplatform for dual modality imaging. The nanoplatform was prepared by incorporating a radionuclide (⁶⁷Ga) to the core of SPIO NPs. The procedures for the synthesis of ⁶⁷Ga-incorporated SPIO NPs and the following surface functionalization are illustrated in Figure 1. In the procedures, we adopted a size-exclusion centrifugation technique to expedite the separation and purification of nanoparticles, which typically takes less than 10 h rather than days if using dialysis tubes or lengthy column separation as in the preparation of SPIO NPs.

Coating the SPIO magnetic particles with a gold shell renders the nanoparticle surface additional tunability because the gold surface can be conveniently functionalized with thiolated molecules.¹⁹ A gold layer was deposited onto the surface using previously reported iterative hydroxylamine seeding process by first mixing the ⁶⁷Ga-incorporated iron oxide seeds with citrate and then aliquots of hydroxylamine and HAuCl₄.^{19,20} The surface modification of the obtained Fe@Au NPs was carried out by anchoring the two thiol groups of lipoic acid on the gold shell, which imparts water solubility and further tunability to the nanoplatform by the peripheral carboxylate groups. The characteristic UV-vis spectra of the Fe@Au NPs (SP: 520 nm) was a sensitive indicator of the Au shell functionalization procedures (Figs. 4 and 5). The polyarginine cell permeation peptide, NH₂GR11, was reported with a high affinity to human prostate cell lines.²¹ In this study, it was chosen to increase the uptake efficiency of Fe@Au NPs into PC-3 cells.

The integrity of nanoparticles is critically important for their biological applications. A sensitive and reliable method was developed to assess the nanoparticle integrity by using an HPLC system equipped with three different detectors: a Wyatt Mini DAWN light scattering detector for the nanoplatform, a Waters UV2996 PDA for a wide range of UV detection of functional molecules anchored on the nanoplatform surface as well as the particles themselves; and an HPLC radio-detector for the radioisotope. From the three HPLC readouts, we can convincingly and accurately determine the integrity of Fe@Au NP-based nanoconjugates. In addition, this HPLC method can be used to monitor the chemical reactions in Figure 1 and the separation/purification procedures.

Uptake of Fe@Au NPs by PC-3 cells shortens the spin-spin relaxation time (*T*₂) by dephasing the spins of neighboring water protons, resulting in darkening *T*₂-weighted images. In the pilot dual-modality imaging study, un-labeled PC-3 cells were used not only as a diluent to mix with different concentrations of labeled cells but also as a control. The dual-modality imaging capabilities of this radioisotope-incorporated Fe@Au nanoplatform was assessed by MRI and autoradiography imaging using both LA-modified Fe@Au NP and NH₂GR11-conjugated Fe@Au NP label PC-3 cells. As seen in Figures 7 and 8, the LA-modified Fe@Au NP labeled cells could be clearly visualized by both MRI and autoradiography imaging if the labeled cell concentrations were above 1 × 10⁵ and 5 × 10⁴ cells/mL, respectively. The cell permeation peptide, NH₂GR11, could enhance the dual-modality detection sensitivity by 2–3 times. It is noteworthy that the incorporated ⁶⁷Ga radioactivity, which is a dominant factor influencing the detection sensitivity of nuclear imaging, was not evaluated as a variable in this pilot study but it can be conveniently increased to improve the sensitivity if the

need arises. Through conjugation with targeting molecules, the LA-modified Fe@Au nanoplatfom may find applications in targeted cancer imaging or therapy.

In summary, our preliminary data clearly demonstrates the potential of using the radioisotope-incorporated Fe@Au NPs for non-invasive dual-modality imaging detection of tumor cells. The significantly improved sensitivity by a cell permeation peptide conjugation and the radioisotope incorporation is a highly desirable property of imaging probes for the systemic detection of cancer metastases, and cell trafficking *in vivo*.

Acknowledgments: This work was partially supported by the USAMRMC Prostate Cancer Research Program (W81XWH-05-1-0592. Xiankai Sun), the NIH Small Animal Imaging Research Program (NCI U24 CA126608. V. D. K.) and a 2005 Society of Nuclear Medicine Pilot Research Award (Xiankai Sun). The MR investigations were performed at the Advanced Imaging Research Center, an NIH BRTP facility (P41RR02584).

References and Notes

- B. Driehuys, Chemistry: Toward molecular imaging with xenon MRI. *Science* 314, 432 (2006).
- K. Goeb, D. G. Engehausen, F. S. Krause, H. P. Hollenbach, G. Niedobitek, M. Buettner, P. Frangou, and K. Engelhard, MRI spectroscopy in screening of prostate cancer. *Anticancer Res.* 27, 687 (2007).
- M. Graefe, D. Stibenz, T. Dietrich, U. Thanabalasingam, P. Stawowy, Z. Yu, E. Nagel, and K. Graf, Magnetic and biological properties of MRI contrast agents for molecular imaging. *Eur. Heart J.* 26, 339 (2005).
- M. A. Haider, T. H. van der Kwast, J. Tanguay, A. J. Evans, A. T. Hashmi, G. Lockwood, and J. Trachtenberg, Combined T2-weighted and diffusion-weighted MRI for localization of prostate cancer. *Am. J. Roentgenol.* 189, 323 (2007).
- M. Kresse, S. Wagner, D. Pfefferer, R. Lawaczek, V. Elste, and W. Semmler, Targeting of ultrasmall superparamagnetic iron oxide (USPIO) particles to tumor cells *in vivo* by using transferrin receptor pathways. *Magn. Reson. Med.* 40, 236 (1998).
- H. Utsumi, K. Yamada, K. Ichikawa, K. Sakai, Y. Kinoshita, S. Matsumoto, and M. Nagai, Simultaneous molecular imaging of redox reactions monitored by overhauser-enhanced MRI with 14N- and 15N-labeled nitroxyl radicals. *Free Rad. Res.* 40, S167 (2006).
- Z. Wang, Q. J. Wu, W. R. Lee, and F. Yin, Three-dimensional MRI and cone-beam CT matching for localization of prostate cancer treatment. *Med. Phys.* 34, 2379 (2007).
- R. Weissleder and M. J. Pittet, Imaging in the era of molecular oncology. *Nature* 452, 580 (2008).
- R. D. Hoge, M. A. Franceschini, R. J. M. Covolan, T. Huppert, J. B. Mandeville, and D. A. Boas, Simultaneous recording of task-induced changes in blood oxygenation, volume, and flow using diffuse optical imaging and arterial spin-labeling MRI. *Neuroimage* 25, 701 (2005).
- T. A. Larson, J. Bankson, J. Aaron, and K. Sokolov, Hybrid plasmonic magnetic nanoparticles as molecular specific agents for MRI/optical imaging and photothermal therapy of cancer cells. *Nanotechnol.* 18 (2007).
- V. Saxena, I. Gonzalez-Gomez, and W. E. Laug, A noninvasive multimodal technique to monitor brain tumor vascularization. *Phys. Med. Biol.* 52, 5295 (2007).
- F. Cicchetti, R. E. Gross, J. W. M. Bulte, M. Owen, I. Chen, M. Saint-Pierre, X. K. Wang, M. X. Yu, and A. L. Brownell, Dual-modality *in vivo* monitoring of subventricular zone stem cell migration and metabolism. *Contr. Med. Mol. Imaging* 2, 130 (2007).
- S. M. Eschmann, D. Schillina, C. Pfannenberger, A. Rieger, M. P. Lichy, C. D. Claussen, R. Bares, A. Stenzl, A. G. Anastasiadis, and H. P. Schlemmer, Clinical staging and re-staging in prostate cancer: Comparison of 11C-Choline-PET/CT and whole body MRI. *Eur. Urol. Suppl.* 6, 89 (2007).
- T. Yamaguchi, J. Lee, H. Uemura, T. Sasaki, N. Takahashi, T. Oka, K. Shizukuishi, H. Endou, Y. Kubota, and T. Inoue, Prostate cancer: A comparative study of C-11-choline PET and MR imaging combined with proton MR spectroscopy. *Eur. J. Nucl. Med. Mol. Imaging* 32, 742 (2005).
- M. S. Judenhofer, H. F. Wehrl, D. F. Newport, C. Catana, S. B. Siegel, M. Becker, A. Thielscher, M. Kneilling, M. P. Lichy, M. Eichner, K. Klingel, G. Reischl, S. Widmaier, M. Rocken, R. E. Nutt, H. J. Machulla, K. Uludag, S. R. Cherry, C. D. Claussen, and B. J. Pichler, Simultaneous PET-MRI: A new approach for functional and morphological imaging. *Nature Med.* 14, 459 (2008).
- B. J. Pichler, H. F. Wehrl, and M. S. Judenhofer, Latest advances in molecular imaging instrumentation. *J. Nucl. Med.* 49, 5S (2008).
- S. J. DeNardo, G. L. DeNardo, A. Natarajan, L. A. Miers, A. R. Foreman, C. Gruettner, G. N. Adamson, and R. Ivkov, Thermal dosimetry predictive of efficacy of In-111-ChL6 nanoparticle AMF-induced thermoablative therapy for human breast cancer in mice. *J. Nucl. Med.* 48, 437 (2007).
- C. A. Boswell, X. K. Sun, W. J. Niu, G. R. Weisman, E. H. Wong, A. L. Rheingold, and C. J. Anderson, Comparative *in vivo* stability of copper-64-labeled cross-bridged and conventional tetraazamacrocyclic complexes. *J. Med. Chem.* 47, 1465 (2004).
- J. L. Lyon, D. A. Fleming, M. B. Stone, P. Schiffer, and M. E. Williams, Synthesis of Fe oxide core/Au shell nanoparticles by iterative hydroxylamine seeding. *Nano Lett.* 4, 719 (2004).
- H. Y. Park, M. J. Schadt, L. Wang, I. I. S. Lim, P. N. Njoki, S. H. Kim, M. Y. Jang, J. Luo, and C. J. Zhong, Fabrication of magnetic core@shell Fe oxide@Au nanoparticles for interfacial bioactivity and bio-separation. *Langmuir* 23, 9050 (2007).
- J. Zhou, J. Fan, and J. T. Hsieh, Inhibition of mitogen-elicited signal transduction and growth in prostate cancer with a small peptide derived from the functional domain of DOC-2/DAB2 delivered by a unique vehicle. *Cancer Research* 66, 8954 (2006).
- Z. Gao, A. N. Lukyanov, A. R. Chakilam, and V. P. Torchilin, PEG-PE/phosphatidylcholine mixed immunomicelles specifically deliver encapsulated taxol to tumor cells of different origin and promote their efficient killing. *J. Drug Target* 11, 87 (2003).
- M. Jones and J. Leroux, Polymeric micelles—a new generation of colloidal drug carriers. *Eur. J. Pharm. Biopharm.* 48, 101 (1999).
- V. P. Torchilin, Polymer-coated long-circulating microparticulate pharmaceuticals. *J. Microencapsul.* 15, 1 (1998).
- V. P. Torchilin, Structure and design of polymeric surfactant-based drug delivery systems. *J. Control. Release* 73, 137 (2001).
- E. V. Groman, J. C. Bouchard, C. P. Reinhardt, and D. E. Vaccaro, Ultrasmall mixed ferrite colloids as multidimensional magnetic resonance imaging, cell labeling, and cell sorting agents. *Bioconjugate Chem.* 18, 1763 (2007).
- E. A. Schellenberger, D. Hogemann, L. Josephson, and R. Weissleder, Annexin V-CLIO: A nanoparticle for detecting apoptosis by MRI. *Acad. Radiol. Suppl.* 2, S310 (2002).
- K. V. P. M. Shafi, A. Ulman, A. Dyal, X. Z. Yan, N. L. Yang, C. Estournes, L. Fournes, A. Wattiaux, H. White, and M. Rafailovich, Magnetic enhancement of gamma-Fe₂O₃ nanoparticles by sonochemical coating. *Chem. Mater.* 14, 1778 (2002).
- P. Wunderbaldinger, L. Josephson, and R. Weissleder, Crosslinked iron oxides (CLIO): A new platform for the development of targeted MR contrast agents. *Acad. Radiol. Suppl.* 2, S304 (2002).

30. P. Wunderbaldinger, L. Josephson, and R. Weissleder, Tat peptide directs enhanced clearance and hepatic permeability of magnetic nanoparticles. *Bioconjugate Chem.* 13, 264 (2002).
31. M. Zhao, M. F. Kircher, L. Josephson, and R. Weissleder, Differential conjugation of tat peptide to superparamagnetic nanoparticles and its effect on cellular uptake. *Bioconjugate Chem.* 13, 840 (2002).
32. M. G. Harisinghani, J. Barentsz, P. F. Hahn, W. M. Deserno, S. Tabatabaei, C. H. van de Kaa, J. de la Rosette, and R. Weissleder, Noninvasive detection of clinically occult lymph-node metastases in prostate cancer. *N. Engl. J. Med.* 348, 2491 (2003).
33. D. M. Koh, G. J. Cook, and J. E. Husband, New horizons in oncologic imaging. *N. Engl. J. Med.* 348, 2487 (2003).

Received: 18 August 2008. Accepted: 4 September 2008.

Gold nanotags for combined multi-colored Raman spectroscopy and x-ray computed tomography

Ming Xiao^{1,2,5}, James Nyagilo^{3,5}, Veera Arora²,
Padmakar Kulkarni², Dongsheng Xu¹, Xiankai Sun^{2,4}
and Digant P Dave^{3,4,6}

¹ College of Chemistry and Molecular Engineering, Peking University, Beijing 100871, People's Republic of China

² Department of Radiology, University of Texas Southwestern Medical Center, Dallas, TX 75390, USA

³ Department of Bioengineering, University of Texas at Arlington, Arlington, TX 76019, USA

⁴ Advanced Imaging Research Center, University of Texas Southwestern Medical Center, Dallas, TX 75390, USA

E-mail: ddave@uta.edu

Received 24 August 2009, in final form 23 October 2009

Published 7 December 2009

Online at stacks.iop.org/Nano/21/035101

Abstract

Multi-color gold-nanoparticle-based tags (nanotags) are synthesized for combined surface-enhanced Raman spectroscopy (SERS) and x-ray computed tomography (CT). The nanotags are synthesized with quasi-spherical gold nanoparticles encoded with a reporter dye (color), each with a unique Raman spectrum. A library of nanotags with six different colors were synthesized for a range of gold nanoparticle sizes and an optimum size has been established to yield the largest SERS intensity and x-ray attenuation that is higher than the iodinated CT contrast agents used in clinics. Proof-of-principle *in vivo* imaging results with nanotags are presented that, for the first time, demonstrates the combined *in vivo* dual modality imaging capability of SERS and CT with a single nanoparticle probe.

 Supplementary data are available from stacks.iop.org/Nano/21/035101/mmedia

(Some figures in this article are in colour only in the electronic version)

1. Introduction

Development of nanoparticle-based contrast agents for diagnostic imaging applications is currently a very active area of research. Over the past decade, a wide variety of materials have been used to synthesize nanoparticle-based contrast agents/beacons for *in vitro* and *in vivo* imaging applications [1–3]. Although many different types (geometry and material) of nanoparticles have shown promising results for imaging in an *in vitro* setting, using them *in vivo* is limited by the constraints related to size, shape, surface chemistry and cytotoxicity. Given these constraints, only a small set of nanoparticles have the potential to be used for *in vivo*

diagnostic imaging applications. Metal nanoparticles have been exploited to enhance contrast of imaging modalities which include MRI [4–8], CT [9–15], photo-acoustic [16, 17] and optical [18–22]. Furthermore, metal nanoparticles exhibit unique electromagnetic properties such as enhanced fluorescence and Raman scattering that can be exploited to improve sensitivity and enable multiplexed imaging [22]. Gold nanoparticles (AuNPs) in particular are well suited for *in vivo* imaging applications given their low toxicity [23] and reactive surface that is conducive for bioconjugation using thiol chemistry. AuNPs provide a robust platform for the development of contrast agents for diagnostic imaging applications.

A multimodality imaging platform can combine the complementary strengths of different imaging modalities to

⁵ Authors contributed equally.

⁶ Author to whom any correspondence should be addressed.

enable comprehensive diagnostic imaging for pathologies such as cancer [24]. Imaging modalities such as CT and MRI enable whole-body imaging with high resolution but lack the sensitivity that can be achieved by optical techniques which in turn have limited penetration depth and interrogation volume. Recognizing the weak endogenous contrast in tissue, a major research focus area in recent years has been the development of exogenous contrast agents to substantially improve molecular and morphological contrast for diagnostic imaging. Even *ex vivo* examination of tissue samples requires staining with multiple contrast agents to obtain a comprehensive morphological and molecular profile for accurate clinical diagnosis. A nanoparticle probe that can simultaneously enhance the contrast for CT and optical imaging in the near-infrared (NIR) can potentially be very valuable for many diagnostic imaging applications. The NIR window of the optical spectrum is preferred for *in vivo* tissue imaging due to substantially lower auto-fluorescence of tissue and deeper penetration of NIR light. The dual modality approach for combined MRI and fluorescence imaging using an iron oxide nanoparticle platform has recently been demonstrated [25–27].

Raman spectroscopy is a highly sensitive optical technique for chemical analysis since each chemical entity has a unique Raman spectrum. A major weakness of Raman spectroscopy is the poor efficiency of Raman scattering which has limited its use in biomedical applications. The efficiency of Raman scattering can dramatically increase (enhancement factor of 10^6 – 10^{14}) when a molecule of interest is in close proximity to a nanosurface via a phenomenon known as surface-enhanced Raman scattering (SERS) [28–32]. With such a large enhancement of Raman scattering, the use of SERS for imaging applications is an attractive alternative to fluorescence. Fluorescent tags have emerged as the dominant optical contrast agents for a wide variety of *in vitro* applications. *In vivo* applications of fluorescent dyes are limited by the auto-fluorescence of tissue. Recently developed near-infrared fluorescent dyes do reduce the auto-fluorescence but fluorescence tags still fundamentally suffer from photobleaching that makes quantification difficult and limited colors (two or three) that can be simultaneously detected due to spectral overlap. These limitations can be overcome by SERS to achieve the detection sensitivity that potentially exceeds that of fluorescence techniques and also achieve quantitative multiplexed detection of several biomolecules simultaneously.

Despite the unique advantages offered by SERS, lack of signal reproducibility and quantification have prevented its widespread use for *in vitro* or *in vivo* imaging applications until now. The lack of signal reproducibility can occur due to the variation in nanoparticle size and shape or aggregation. Metal nanoparticles tend to aggregate in commonly used buffers and serum. Although aggregation substantially enhances SERS, from an imaging or sensing application standpoint it is undesirable since aggregation cannot be controlled, the resultant SERS signal fluctuates and typically the aggregate size is too large to be used for any *in vivo* applications. Recently a promising design strategy to synthesize nanotags for SERS was developed [19, 20, 33]. The design involves encapsulating organic dyes as signature reporter dyes between

AuNP and a layer of silica or polyethylene glycol (PEG) which prevents the AuNPs from aggregating. These nanotags, each with a unique Raman spectrum (color), can be utilized as beacons for imaging with target ligands attached to the PEG or silica surface with well-established bioconjugation chemistries.

CT is a widely used imaging modality for various clinical diagnostic applications. Hard tissues have higher x-ray attenuations than various soft tissues whereas the contrast between soft tissues is inherently poor, which limits the sensitivity with which diagnosis of pathologies such as cancer can be made. Currently, iodine-based compounds are used to enhance the contrast of CT which have the limitations of a short imaging window due to rapid clearance by kidneys and renal toxicity. Metals such as gold have a higher x-ray attenuation coefficient due to their high electron density and atomic number compared to conventionally used iodine compounds. Nanoparticle-based CT contrast agents have been reported for *in vivo* imaging, which include bare AuNPs [11], polymer-coated AuNPs [12], gadolinium-coated AuNPs [13] and polymer-coated Bi_2S_3 [14]. Molecular CT imaging of cancer using targeted AuNPs in cell culture was recently demonstrated by Popovtzer *et al* [15].

In this paper we report the first proof-of-principle demonstration of dual modality probes for combined CT and SERS imaging. The multi-color hybrid nanotags are quasi-spherical gold nanoparticles coated with Raman reporter dyes (color) encapsulated by a monolayer of poly(ethylene) glycol (PEG) molecules with carboxylate functional groups for further bioconjugation with a ligand. We describe nanotag synthesis, quantitative contrast characterization and present results of dual modality *in vivo* imaging.

2. Materials and methods

2.1. Synthesis of AuNPs

The size and shape of metal nanoparticles are critical factors that influence the SERS signal. The enhancement of a given molecular vibration peak in the SERS spectrum depends on the morphology of the metal nanoparticle. In this work, AuNPs of different sizes were employed as the cores to construct nanotags. The AuNPs were synthesized using published methods with modifications [34, 35]. In brief, to prepare citrate-coated AuNPs, an aqueous solution of 0.25 mM HAuCl_4 (50 ml) was first heated to boiling point with constant stirring, to which a certain volume of 1% (wt) sodium citrate (0.40–1.75 ml) was added. Within a minute, the solution turned from faint blue to red, indicating the formation of AuNPs. The boiling and stirring were continued for 30 min. The resulting solution was then cooled down to room temperature, which afforded AuNPs with a mean diameter ranging from 16.7 ± 1.7 to 65.6 ± 6.4 nm as determined by TEM. Particle size and size distribution can be reproducibly controlled by varying the volume of the sodium citrate solution added. To synthesize AuNPs of larger diameters (80–120 nm) a seed growth method was used [35]. In this method AuNPs of different sizes coated with 2-mercaptosuccinic acid (MSA) were synthesized by

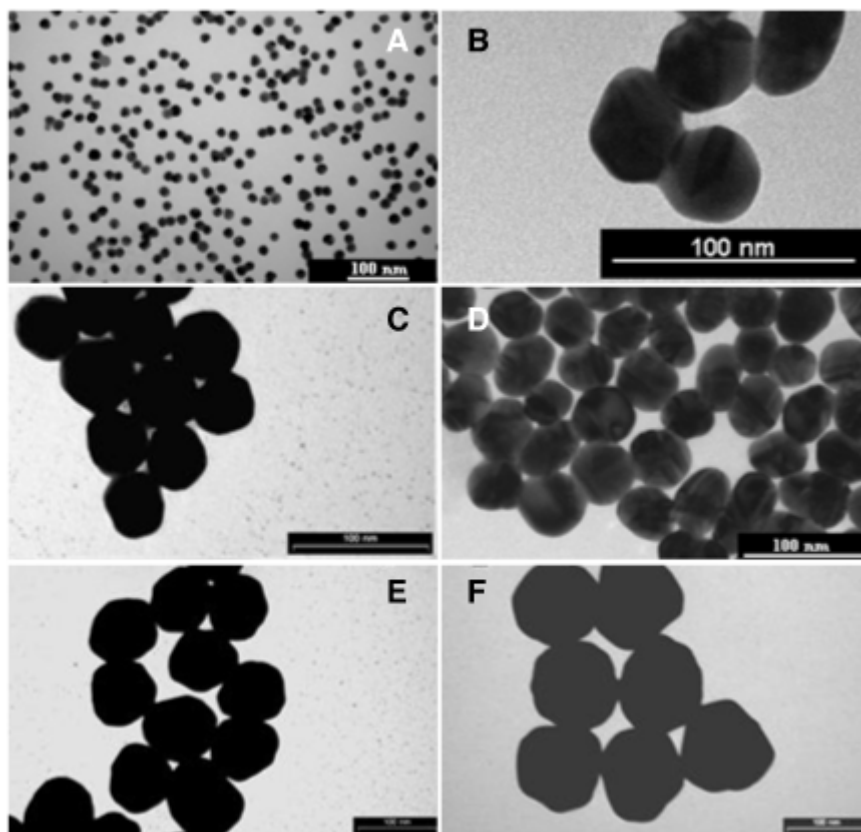


Figure 1. TEM images of quasi-spherical AuNPs of various sizes: (A) 16.7 ± 1.7 nm, (B) 43.9 ± 3.8 nm, (C) 51 ± 3.1 nm, (D) 65.6 ± 6.4 nm, (E) 83 ± 5.1 nm and (F) 114 ± 7.9 nm. The measured ‘diameter’ represents an average of 300 particles. The ‘diameter’ is quantified by a circle circumscribing individual quasi-spherical AuNPs.

adding different amounts of the smallest citrate-coated AuNPs (16.7 ± 1.7 nm) to a solution containing MSA and HAuCl₄ at a fixed molar ratio under rigorous stirring. The color change of the reaction mixture (pink to purple) reflects the growth of AuNPs.

2.2. Morphological characterization of AuNPs

The synthesized AuNPs ranging from 20 to 120 nm are shown in figure 1. Morphological characterization of AuNPs was done with transmission electron microscopy (TEM) and dynamic light scattering (DLS) measurements. All synthesized particles are mono-dispersed and quasi-spherical in shape (figure 1). The average ‘diameter’ estimation of the quasi-spherical AuNPs from the TEM images ($n = 300$) is done by circumscribing a circle over an AuNP. The hydrodynamic size of the AuNPs estimated by DLS measurement is lower by 10–25% for different sizes compared to TEM measurement due to the fact that the nanoparticles are non-spherical.

2.3. Synthesis of multi-color nanotags

Coating of a Raman reporter dye on synthesized AuNPs is achieved using the method described by Qian *et al* [18]. A freshly prepared Raman reporter dye solution was added to a mono-dispersed quasi-spherical AuNP solution ($1.1 \times$

10^{10} particles ml^{-1}) with the final concentration ranging from 5 to 15 μM . The ratio of the dye to AuNPs varies for different dyes. The optimum ratio was determined for each Raman reporter dye which yields maximum coverage of the dye on the surface of AuNPs without resulting in aggregation. The rate of addition and speed of mixing were also found to be critical in obtaining optimum coverage of the dye as reported by others [18]. Raman-reporter-dye-coated AuNPs were PEGylated by a mixture of SH-mPEG (10 μM , MW 5000) and SH-PEG-COOH (1 μM , MW 2000) solutions. Varying the ratio of the mixture does not affect the nanotag stability but does alter the charge. The PEGylation provides steric stabilization, improved biodistribution properties and carboxylate groups for further bioconjugation with biomolecules.

2.4. Nanotag stability

After the dye encoding and PEGylation, the resultant nanotags were again characterized by UV–vis absorption spectroscopy, TEM and DLS measurements to ascertain that they were mono-dispersed and adequately PEGylated while retaining their characteristic SERS spectra. A 3 nm redshift of the plasmon peak of AuNPs was observed as a result from the PEGylation (figure 2(A)). A PEG layer is evidently seen in the TEM images (figure 2(B)) encapsulating the

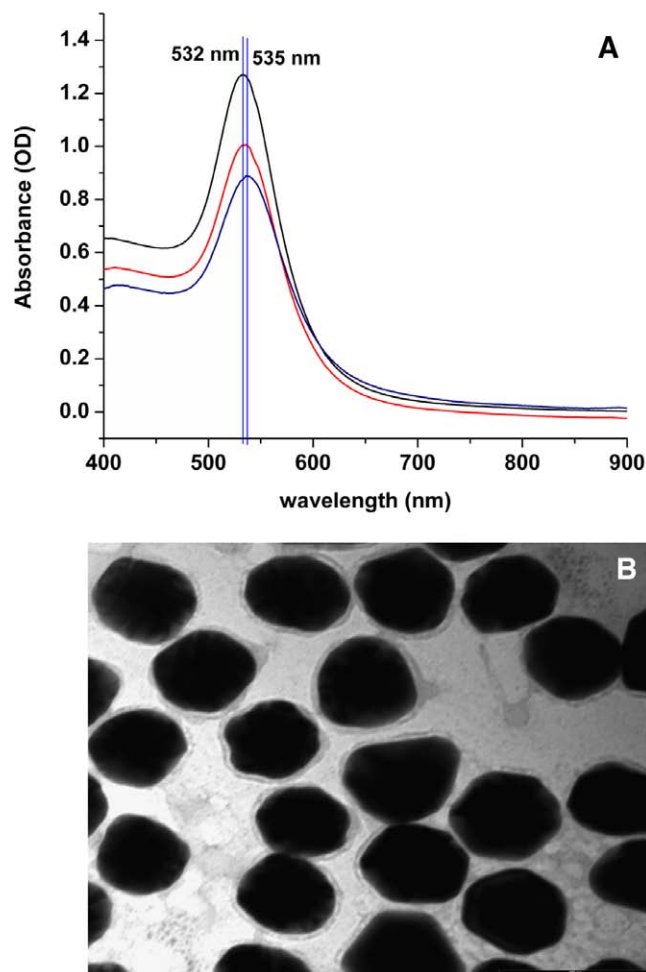


Figure 2. Extinction curves of AuNPs and nanotags which show a 3 nm redshift after PEGylation of the AuNPs (A) and TEM image of nanotags (B) showing the PEG layer encapsulating the AuNPs.

AuNPs. There was minimal broadening of the attenuation curve as measured by the full width at half-maximum of the attenuation curve, which indicates that the nanotags were not aggregated. In addition, virtually no change in size or size distribution was observed on the DLS histograms. Stability of the nanotags was tested in various solvents (PBS, MES, goat serum) (supporting information figure S1, available at stacks.iop.org/Nano/21/035101/mmedia). The nanotag solutions were monitored by UV-vis, DLS and SERS for a month with no signs of aggregation or spectral changes, which attests to the stability of the nanotags.

2.5. Raman spectrum measurement

Raman spectrum measurements of nanotags were made with a home-made Raman spectroscopy module operating in reflection mode. A 785 nm single line laser (Ocean Optics) fiber is coupled to the Raman module. SERS spectra are collected by a microscope objective and recorded by a high resolution spectrometer (Ocean Optics, QE65000). The near-infrared excitation wavelength was chosen to minimize auto-fluorescence from tissue during *in vivo* imaging. The home-

made Raman module is used for all the *in vitro* and *in vivo* measurements.

2.6. X-ray attenuation and CT imaging

X-ray attenuation of the nanotags was quantified by a Siemens Inveon PET-CT Multimodality System (Knoxville, TN). CT images were obtained at 80 kV and 500 mA with a focal spot of 58 μm on the Siemens Inveon PET-CT scanner. The total rotation of the gantry was 360° with 360 rotation steps obtained at an exposure time of approximately 225 ms/frame. Under low magnification the effective pixel size is 103.03 μm . CT images were reconstructed with a down sample factor of 2 using Cobra reconstruction software. Reconstructed images were analyzed using the Siemens Inveon research workplace (IRW) software.

3. Results and discussion

3.1. SERS characterization

Using different reporter dyes, we have synthesized nanotags of six different colors, each with a unique Raman spectrum. The six different reporter dyes used to synthesize single-colored nanotags are: Cresyl Violet, Rhodamine 6G Tetrafluoroborate, Crystal Violet, DTTC Iodide, Nile Blue and 2-Thiouracil. These first five are laser dyes that are positively charged which readily adsorb to the negatively charged AuNPs whereas 2-Thiouracil binds via the thiol chemistry. None of the dyes exhibit a measurable Raman spectrum in the absence of AuNPs, even at saturation concentrations.

The representative signature Raman spectrum of each color nanotag encoded with a specific Raman reporter dye is shown in figures 3(A)–(E). SERS spectra of 2-Thiouracil-coated nanotags is included in the supporting information (figure S4, available at stacks.iop.org/Nano/21/035101/mmedia). The Raman spectrum of nanotags was recorded while suspended in deionized water. Each color nanotag has a unique spectrum distinguished by the location and magnitude of the various peaks. The locations of some peaks do coincide for different nanotags due to a common vibrational mode of specific chemical bonds but there are a number of others peaks which are unique to each reporter dye. Nanotags of different colors show excellent reproducibility of their respective Raman spectra in terms of the location of the peaks and their relative magnitudes. The absolute magnitudes of the Raman spectrum peaks do vary (10–15%) for different batches of synthesized nanotags but consistently a large Raman enhancement is achieved. The variation in the magnitude of the Raman spectrum is attributed to variation in the amount of dye attached to AuNPs and variation in the size of AuNPs. Shown in figure 3(F) is the SERS signal measured from a mixture of four nanotags. Peaks attributable to a specific reporter dye are clearly identifiable in a mixture of nanotags. Raman transition peaks of specific dyes are tabulated in table 1 (supporting information, available at stacks.iop.org/Nano/21/035101/mmedia).

It is noteworthy that the magnitude of Raman peaks shows a linear dependence on the concentration of the nanotags. This

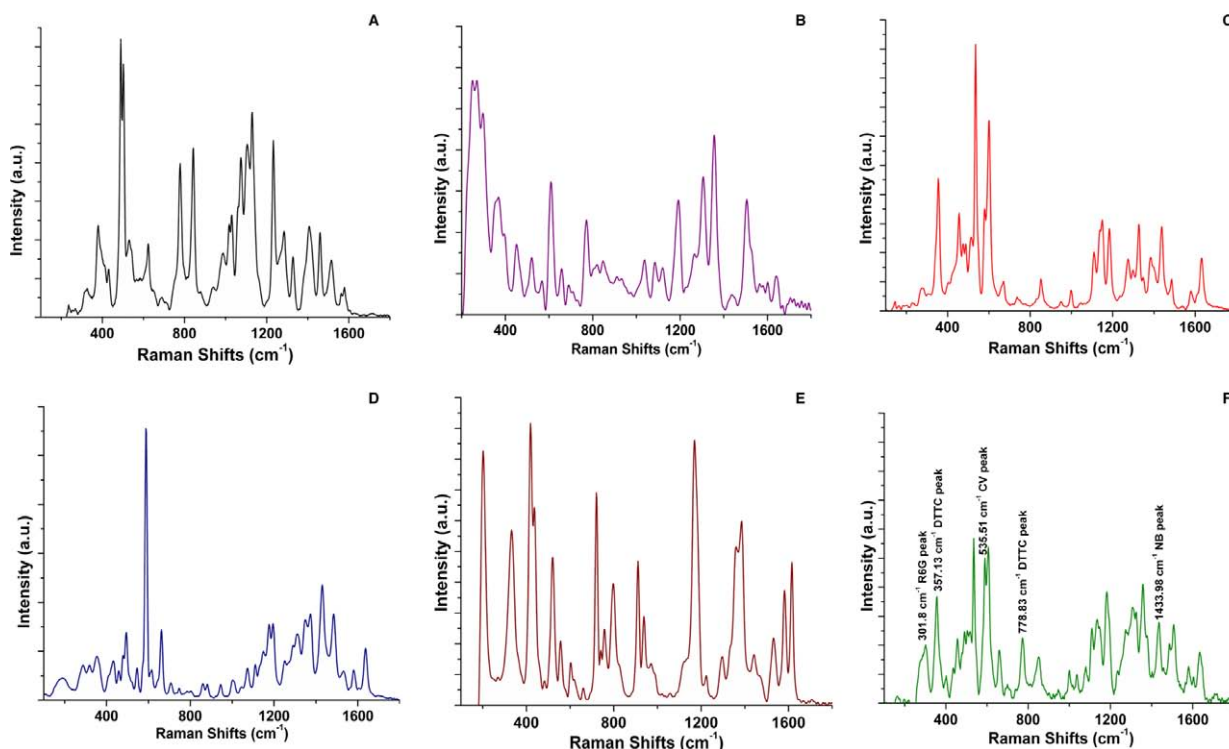


Figure 3. Raman spectra of five different color nanotags: (A) DTTC iodide (DTTC), (B) Rhodamine 6G (R6G), (C) Cresyl violet (CV), (D) Nile blue perchlorate (NB) and (E) Crystal violet. Each color has a unique spectrum distinguished by location and magnitude of the various peaks which clearly enables their identification in mixtures. (F) SERS spectra of a solution containing a mixture of four color nanotags: Rhodamine 6G, DTTC iodide, Cresyl violet and Nile blue.

is critically important for quantitative SERS imaging. The measurement dynamic range of nanotag detection is greater than 30 dB, which represents a concentration range from 10 pM to 10 nM. Nanotags were synthesized from AuNPs of various sizes (20–120 nm) and their Raman spectra were recorded. The largest Raman enhancement was obtained for nanotags synthesized with AuNPs with a diameter of 65.6 ± 6.4 nm. Compared to nanotags synthesized with commercially available spherical AuNPs of similar size, the ones prepared with our quasi-spherical AuNPs yield 2–3 times (depending on the peak compared) higher SERS intensity as reflected in the Raman spectrum (supporting information figure S3, available at stacks.iop.org/Nano/21/035101/mmedia). Since DTTC nanotags fluoresce at the excitation wavelength, they provide a good opportunity to compare fluorescence and SERS. The fluorescence intensity of DTTC is also enhanced due to the AuNPs (surface-enhanced fluorescence) and the SERS signal is further enhanced due to the resonant effect since the absorption peak (795 nm) of DTTC is close to the laser excitation wavelength. Shown in figure 4 is the combined fluorescence and SERS DTTC spectra. Magnitudes of both spectra are comparable, which indicates the large Raman enhancement. For comparison, the scaled fluorescence spectrum of neat DTTC is also shown. The SERS intensity remains stable as a function of time upon excitation whereas the fluorescence signal decays with increasing exposure time. The stability of SERS signal is a critical advantage over fluorescence measurements for quantitative analysis.

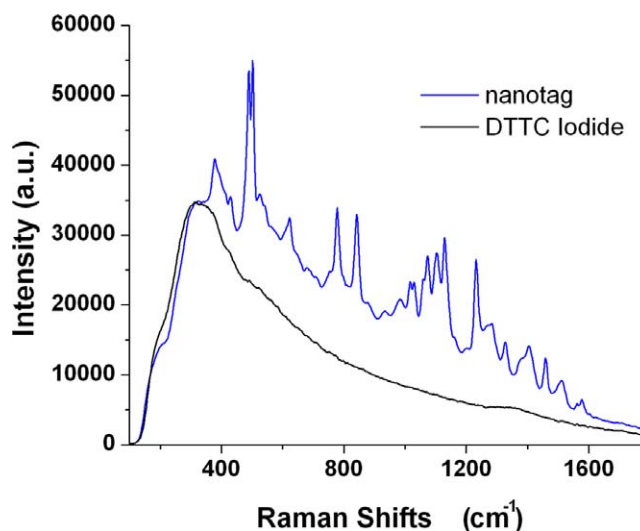


Figure 4. Combined SERS and surface-enhanced fluorescence spectra of DTTC iodide (blue color). Scaled fluorescence spectra of neat DTTC iodide (black color) is shown for comparison.

3.2. CT contrast

Nanotags of two sizes (65.6 ± 6.4 nm and 43.9 ± 3.8 nm) which show the largest SERS intensity from the range of various sizes were chosen for x-ray attenuation characterization. Vials containing serially diluted nanotags were placed in the CT

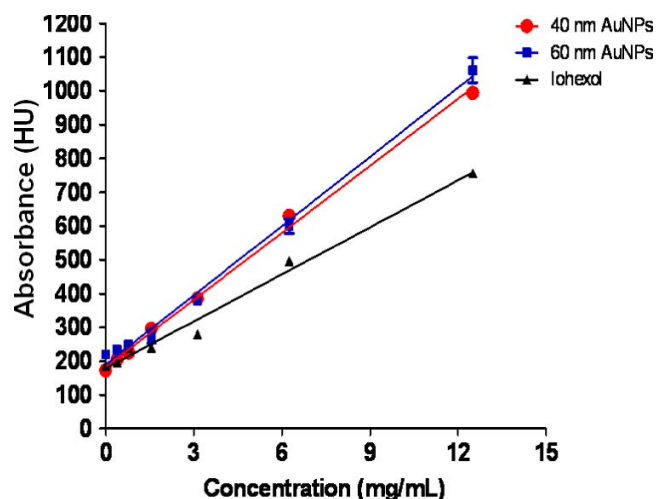


Figure 5. Measured x-ray attenuation of AuNPs (40 and 60 nm) and Iohexol as a function of their concentration. The offset in the plots is due to the x-ray attenuation in the plastic vials used to hold the solution for the measurements.

scanner. The measured x-ray attenuation values of nanotags show a linear dependence on the nanotag concentration (figure 5). The offset in the plots is due to the background x-ray attenuation of the plastic vials used to hold the samples. Next, the x-ray attenuation of the nanotags is compared to Iohexol (Omnipaque™, GE Healthcare), an iodine-based clinical CT contrast agent. As shown in figure 5, both nanotags' (65.6 ± 6.4 nm and 43.9 ± 3.8 nm) size range must be present for CT contrast and, afford higher CT contrast than Iohexol at the same concentrations (molar equivalent of gold versus iodine). These values are slightly higher than the ones reported by Xu *et al* for AuNPs of comparable sizes [36].

3.3. *In vivo* CT contrast of nanotags

All *in vivo* animal imaging studies were performed in compliance with guidelines set by the University of Texas Southwestern Institutional Animal Care and Use Committee. To demonstrate *in vivo* CT contrast of the nanotags, three Balb/c mice were fasted overnight and scanned under 2% isoflurane anesthesia for the duration of the imaging before receiving $100 \mu\text{l}$ of 12.5 mg ml^{-1} of the 65.6 ± 6.4 nm nanotags via the tail vein. At 24 h post-injection, the mice were sedated and scanned again. Each CT scan time was approximately 6 min. As shown in figure 6, the spleen became clearly visible with the AuNP-based nanotags as contrast agent. The image quantification revealed that the CT attenuation value was 432 HU in the spleen at 24 h post-injection, while it was around 100 HU in other soft tissues. The presence of nanotags in the spleen was further confirmed by TEM images of the spleen tissue slices. In addition, the TEM images showed that the nanotags were internalized in the spleen cells and preferentially accumulated in the endosomes (figure 7). This observation is consistent with recently published work [37] and demonstrates the *in vivo* stability of the AuNP-based nanotags.

3.4. Combined *in vivo* SERS and CT imaging

To demonstrate the dual contrast of SERS and CT of our nanotags *in vivo*, three nude mice were injected with $100 \mu\text{l}$ of the 65 nm nanotags at a concentration of 12.5 mg ml^{-1} subcutaneously after sedation under 2% isoflurane anesthesia. SERS and CT scans were recorded pre- and post-injection. The SERS images were recorded followed by CT scanning. For SERS imaging, the sedated mouse was placed on a platform and its body temperature was maintained by a water-circulation heating pad. The SERS spectra were acquired with a $10\times$ (0.25 N.A.) microscope objective with an integration time of 8 s and incident power of 10 mW. Recorded SERS spectra before and after injection of nanotags are shown in figures 8(A) and (B), respectively. Representative whole-body CT images of the mice before and after the nanotag injection are shown in figures 8(C) and (D), respectively. The *in vivo* pre-injection Raman spectrum is magnified ($6\times$) to clearly visualize the Raman peaks of the tissue. The *in vivo* Raman spectra of the nanotags remains intact with little change or distortion in the peaks and their linewidth. Except for overlapping peaks at 300 and 400 cm^{-1} , the rest can be readily attributed to the reporter dye. Raman spectra of the injected nanotags were also recorded as a function of nanotag concentration. Serially diluted solutions of nanotags were injected subcutaneously at various locations. Due to the rapid diffusion of the nanotags in tissue it is difficult to establish the functional dependence of Raman signal magnitude on the nanotag concentration but nonetheless a strong Raman spectrum was successfully recorded at the lowest concentration of $25 \mu\text{g ml}^{-1}$.

4. Conclusions

We have developed gold-nanoparticle-based nanotags for combined SERS and CT imaging. Dual imaging probes of six different colors were synthesized and characterized, each with a distinct Raman spectrum. The optimal size (65.6 ± 6.4 nm) of quasi-spherical AuNPs has been established to synthesize nanotags that yield the largest enhancement of SERS signals. Nanotags with an AuNP core 40–60 nm in diameter are suitable for *in vivo* dual modality imaging as demonstrated by their large SERS intensity and high CT contrast. Understandably, the magnitude of contrast is not solely dictated by the SERS signal or x-ray attenuation but also by the *in vivo* distribution profile of the nanotags. Smaller nanoparticles usually exhibit better biodistribution properties but ultimately it is the product of the signal magnitude per nanotag and the concentration of the nanotags accumulated at the site of interest that dictates the final imaging contrast. By conjugating targeting molecules specific to a biomarker with the nanotags, desired *in vivo* kinetics and distribution could be achieved to realize targeted dual modality imaging enabled by a single nanoplatform. In perspective, an array of different biomarker targeted nanotags with corresponding colors would provide a non-invasive technique for molecular profiling of diseases such as cancer. In a clinical setting,

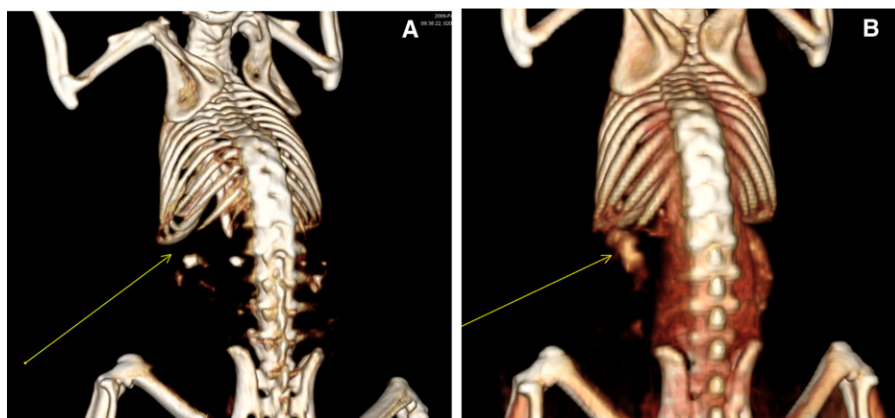


Figure 6. 3D CT images of the mouse before injection of nanotags (A) and 24 h post-injection (B). Yellow arrows indicate the location of the spleen which is not visible without the nanotags while it is clearly revealed on the CT image once the nanotags accumulate in the spleen.

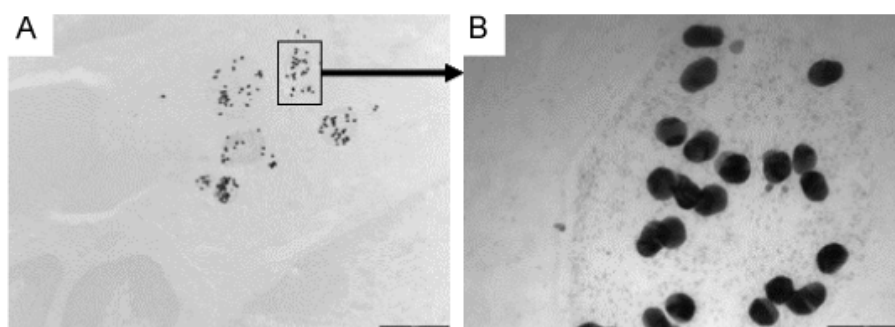


Figure 7. TEM images of spleen tissue showing the accumulation of nanotags ((A) and (B)). The nanotags are internalized in spleen cells and preferentially accumulate in endosomes (B).

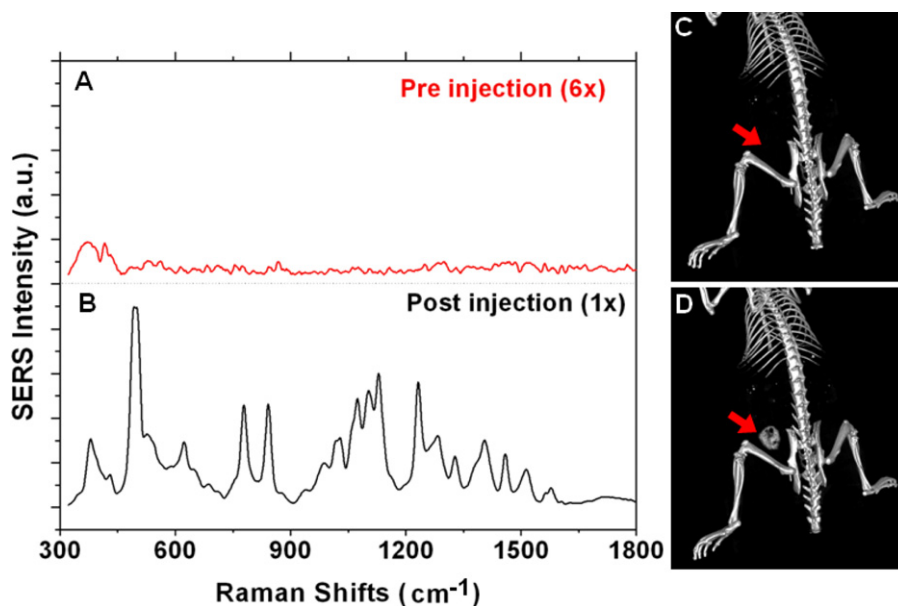


Figure 8. SERS and CT images from subcutaneously injected nanotags (60 nm) in a nude mouse. (A) and (B) are recorded Raman spectra whereas (C) and (D) are 3D CT images pre- and post-injection, respectively. The arrows in panel (C) and (D) point to the site of injection and CT contrast generated.

such nanotags can be potentially used for dual modality imaging of cancer, in which the tumor is first localized by whole-body CT imaging and then assessed by SERS at

the molecular level to obtain the profile of multiple cancer-specific biomarkers for patient-specific diagnosis, staging and treatment.

Acknowledgments

This work was supported in part by DOE (grant no. DE-FG02-O4CH11280) and DOD (grant nos. W81XWH-08-1-0305 and W81XWH-05-1-0592). We thank Michael Long for help with CT imaging and Tiffani Anthony for animal handling and injecting nanotags in mice.

References

- [1] Ferrai M 2005 *Nat. Rev. Cancer* **5** 161–71
- [2] Jaiswal J K and Simon S M 2003 *Nat. Biotechnol.* **21** 47–51
- [3] Michalet X, Pinaud F F, Bentolila L A, Tsay J M, Doose S, Li J J, Sundaresan G, Wu A M, Gambhir S S and Weiss S 2005 *Science* **307** 538–44
- [4] Harisinghani M G, Barentsz J, Hahn P F, Deserno W M, Tabatabaei S, van de Kaa C H, de la Rosette J and Weissleder R 2003 *N. Engl. J. Med.* **348** 2491–9
- [5] Huh Y M et al 2005 *J. Am. Chem. Soc.* **127** 12387–91
- [6] Hadjipanayis C G, Bonder M J, Balakrishnan S, Wang X, Mao H and Hadjipanayis G C 2008 *Small* **11** 1925–9
- [7] Moore A, Marecos E, Bogdanov A Jr and Weissleder R 2000 *Radiology* **214** 568–74
- [8] Lewin M, Carlesso N, Tung C H, Tang X W, Cory D, Scadden D T and Weissleder R 2000 *Nat. Biotechnol.* **18** 410–4
- [9] Kim D, Park S, Lee J H, Jeong Y Y and Jon S 2007 *J. Am. Chem. Soc.* **129** 7661–5
- [10] Hyafil F, Cornily J C, Feig J E, Gordon R, Vucic E, Amirbekian V, Fisher E A, Fuster V, Feldman L J and Fayad Z A 2007 *Nat. Med.* **13** 636–41
- [11] Hainfeld J F, Slatkin D N, Focella T M and Smilowitz H M 2006 *Br. J. Radiol.* **79** 248–53
- [12] Alric C et al 2008 *J. Am. Chem. Soc.* **130** 5908–15
- [13] Cai Q Y, Kim S H, Choi K S, Kim S Y, Byun S J, Kim K W, Park S H, Jung S K and Yoon K H 2007 *Invest Radiol.* **42** 797–806
- [14] Rabin O, Manuel Perez J, Grimm J, Wojtkiewicz G and Weissleder R 2006 *Nat. Mater.* **5** 118–22
- [15] Popovtzer R, Agrawal R A, Kotov N A, Popovtzer A, Balter J, Carey T E and Kopelman R 2008 *Nano Lett.* **8** 4593–6
- [16] Eghtedari M, Liopo A V, Copland J A, Oraevsky A A and Motamedi M 2009 *Nano Lett.* **287–91**
- [17] Wang B, Yantsen E, Larson T, Karpouk A B, Sethuraman S, Su J L, Sokolov K and Emelianov S Y 2009 *Nano Lett.* **9** 216–22
- [18] Qian X, Peng X-H, Ansari D O, Yin-Goen Q, Chen C D, Shin G Z, Yang L, Young A N, Wang M D and Nie S 2008 *Nat. Biotechnol.* **26** 83–90
- [19] Gao X, Cui Y, Levenson R M, Chung L W and Nie S 2004 *Nat. Biotechnol.* **22** 969–76
- [20] Keren S, Zavaleta C, Cheng Z, Zerda A, Gheysens O and Gambhir S S 2008 *Proc. Natl Acad. Sci.* **105** 5844–9
- [21] Cai W, Shin D-W, Chen K, Gheysens O, Cao Q, Wang S X, Gambhir S S and Chen X 2006 *Nano Lett.* **6** 669–76
- [22] Gobin A M, Lee M H, Halas N J, James W D, Drezek R A and West J L 2007 *Nano Lett.* **7** 1929–34
- [23] Shukla R, Bansal V, Chaudhary M, Basu A, Bhonde R R and Sastry M 2005 *Langmuir* **21** 10644–54
- [24] Lennart B and Torkzad M R 2003 *JAMA* **290** 3248–9
- [25] Veiseh O et al 2005 *Nano Lett.* **5** 1003–8 MRI + fluorescence
- [26] Medarova Z, Rashlovetsy L, Pentazopoulos P and Moore A 2009 *Cancer Res.* **69** 1182–89
- [27] Moore A, Medarova Z, Potthast A and Dai G 2004 *Cancer Res.* **64** 1821–7
- [28] Fleischmann M, Hendra P J and McQuillan A J 1974 *Chem. Phys. Lett.* **26** 163–6
- [29] Jeanmaire D L and van Duyne Richard P 1977 *J. Electroanal. Chem.* **84** 1–20
- [30] Albrecht M G and Creighton J A 1977 *J. Am. Chem. Soc.* **99** 5215–9
- [31] Kneipp K, Wang Y, Kneipp H, Perelman L T, Itzkan I, Dasari R R and Feld M S 1997 *Phys. Rev. Lett.* **78** 1667–70
- [32] Nie S and Emory S R 1997 *Science* **275** 1102–6
- [33] Kim J H et al 2006 *Anal. Chem.* **78** 6967–73
- [34] Frens G 1973 *Nat. Phys. Sci.* **241** 20–2
- [35] Niu J L, Zhu T and Liu Z F 2007 *Nanotechnology* **18** 325607
- [36] Xu C, Tung G A and Sun S 2008 *Chem. Mater.* **20** 4167–9
- [37] Nativo P, Prior I A and Brust M 2008 *ACS Nano* **2** 1639–44